

รายงานวิจัยฉบับสมบูรณ์

โครงการ

กลไกการสื่อสารสัญญาณแคลเซียมและการต้านทานความเครียดจากความเค็มในข้าว โดยใช้การวิเคราะห์ทรานคริปโทมและวิธีการเชิงโมเลกุล

Mechanisms of calcium signaling and salt stress tolerance in rice using transcriptomics analysis and molecular approaches

โดย

รศ. ดร. ธีรพงษ์ บัวบูชา ภาควิชาชีวเคมี คณะวิทยาศาสตร์ จุฬาลงกรณ์มหาวิทยาลัย

สัญญาเลขที่ BRG5680019

รายงานวิจัยฉบับสมบูรณ์

โครงการ

กลไกการสื่อสารสัญญาณแคลเซียมและการต้านทานความเครียดจากความเค็มในข้าว โดยใช้การวิเคราะห์ทรานคริปโทมและวิธีการเชิงโมเลกุล Mechanisms of calcium signaling and salt stress tolerance in rice using transcriptomics analysis and molecular approaches

โดย

รศ. ดร. ธีรพงษ์ บัวบุชา ภาควิชาชีวเคมี คณะวิทยาศาสตร์ จุฬาลงกรณ์มหาวิทยาลัย

สนับสนุนโดยสำนักงานกองทุนสนับสนุนการวิจัย

(ความเห็นในรายงานนี้เป็นของผู้วิจัย สกว. ไม่จำเป็นต้องเห็นด้วยเสมอไป)

สารบัญ

| บทคัดย่อ | 4 |
|------------------------|----|
| Abstract | 5 |
| Introduction | 6 |
| Materials and Methods | 9 |
| Results and Discussion | 16 |
| Output | 41 |
| ภาคผนวก | 42 |

บทคัดย่อ

รหัสโครงการ: BRG5680019

ชื่อโครงการ: กลไกการสื่อสารสัญญาณแคลเซียมและการต้านทานความเครียดจากความเค็มในข้าว

โดยใช้การวิเคราะห์ทรานคริปโทมและวิธีการเชิงโมเลกุล

ชื่อนักวิจัย: รองศาสตราจารย์ ดร. ธีรพงษ์ บัวบูชา

ภาควิชาชีวเคมี คณะวิทยาศาสตร์ จุฬาลงกรณ์มหาวิทยาลัย

Email Address: <u>Teerapong.B@Chula.ac.th</u>

ระยะเวลาโครงการ: 3 ปี

การศึกษาโพรไฟล์ทรานสคริปโทมของข้าวขาวดอกมะลิ 105 เปรียบเทียบกับข้าวทรานส์เจนิกที่มียืน OsCam1-1 แสดงออกเกินปกติ พบยืน ที่มีการแสดงออกแตกต่างกันภายใต้ภาวะปกติและภาวะเครียดจากความเค็มจำนวน 1,756 และ 1,190 ยืน ตามลำดับ การวิเคราะห์ Gene Ontology (GO) Enrichment ของยืนตอบสนองต่อความเครียดจากความเค็มที่มีระดับการ แสดงออกเพิ่มขึ้นในข้าวทรานส์เจนิก พบว่า GO term ที่เกี่ยวกับ carbohydrate metabolic process, protein phosphorylation, response to water, regulation of transcription และ lipid transport เพิ่มขึ้น การแสดงออกของยืนที่ แสดงออกแตกต่างกันถูกยืนยันด้วยวิธี real-time RT-PCR ได้แก่ ยีนที่สร้าง transcription factor AP2, β-amylase, isocitrate lyase, malate synthase, aconitase, ERD1, และ glycosyl hydrolase การวิเคราะห์วิถีด้วย Mapman พบยีนที่มีการ แสดงออกสูงขึ้นในข้าวทรานส์เจนิกจำนวนมากอยู่ในวิถีที่เกี่ยวข้องกับทรานสคริปชัน การย่อยน้ำตาลและแป้ง ไกลโคลิซิส วัฏจักร TCA และวัฏจักรไกลออกซิเลต แสดงให้เห็นว่าการแสดงออกเกินปกติของ OsCam1-1 อาจส่งผมต่อเมแทบอลิซึมของ คาร์โบไฮเดรตในข้าวที่ปลูกภายใต้ภาวะเครียดจากความเค็ม นอกจากนี้พบว่าการแสดงออกของยีน OsICL ซึ่งสร้างเอนไซม์ไอโซชิ เทรตไลเอสมีระดับการแสดงออกที่เพิ่มขึ้นในข้าวทรานส์เจนิกทั้งสามสายพันธุ์ทั้งที่ปลูกในภาวะปกติและภาวะเครียดจากความเค็ม ยีน OsICL จึงเป็นยีนเป้าหมายที่น่าสนใจในการศึกษาเพิ่มเติมต่อไป

ก่อนหน้านี้เราระบุโปรตีนเป้าหมายของ OsCaM1 และโปรตีนคล้าย CaM ชนิดหนึ่งคือ OsCML3 จากข้าวโดยวิธี cDNA expression library screening โปรตีนเป้าหมายหนึ่งของ OsCaM1 คือโปรตีน Myosin heavy chain like (MHCL) ในงานวิจัย นี้ได้ยืนยันการจับกันระหว่าง OsCaM1 และ OsMHCL ด้วยวิธี pull-down ในภาวะที่มีแคลเซียม นอกจากนี้ yeast two-hybrid ยังแสดงให้เห็นว่า OsMHCL สามารถจับกับโปรตีนคล้าย CaM สามชนิดคือ OsCML4, OsCML5 และ OsCML8 ทั้งในภาวะที่มี แคลเซียมและไม่มีแคลเซียมได้อีกด้วย สำหรับการศึกษาโปรตีนเป้าหมายของ OsCML3 และโปรตีนอนุพันธ์ที่ไม่มีปลาย C-terminal (OsCML3m) พบว่าโปรตีนทั้งสองชนิดแสดงสมบัติการจับแคลเซียมและการเปลี่ยนแปลงโครงรูปหลังการจับแคลเซียม แต่เฉพาะ OsCML3m เท่านั้นที่พบว่าสามารถจับเพปไทด์เป้าหมาย CaM kinase แได้ การศึกษาการเปลี่ยนโครงสร้างทุติยภูมิ เมื่อจับแคลเซียมด้วยวิธี CD พบว่า OsCML3m มีปริมาณ α-helix สูงกว่า OsCML3 ในการศึกษา localization พบ OsCML3 อยู่ที่เยื่อหุ้มเชลล์ แต่พบ OsCML3m ในนิวเคลียส ก่อนหน้านี้เราสามารถระบุโปรตีนเป้าหมายหนึ่งของ OsCML3 ได้ คือ high mobility group B1 (OsHMGB1) ในการศึกษาด้วยวิธี bimolecular fluorescence complementation analysis พบว่า OsHMGB1 จับกับ OsCML3, OsCML3m และ OsCML3s (ซิสเทอินถูกเปลี่ยนไปเป็นเซรีนในบริเวณ prenylation) ในนิวเคลียส เป็นการยืนยันว่า OsHMGB1 เป็นโปรตีนเป้าหมายในพีชจริง การศึกษาผลของ OsCML3 หรือ OsCML3m ต่อการจับกับดีเอ็นเอ ของ OsHMGB1 พบว่า OsCML3 ไม่มีผล เมื่อพิจารณาผลการทดลองทั้งหมดร่วมกันพบว่า OsCML3 น่าจะมีหน้าที่ควบคุมการจับดีเอ็นเอของ OsHMGB1 ในนิวเคลียส และ ปลาย C-terminal น่าจะทำหน้าที่เป็นตัวควบคุม

คำสำคัญ คัลมอดุลิน ทรานสคริปโทม ข้าว

Abstract

Project Code: BRG5680019

Project Title: Mechanisms of calcium signaling and salt stress tolerance in rice using

transcriptomics analysis and molecular approaches

Investigator: Teerapong Buaboocha, Ph.D.

Department of Biochemistry, Faculty of Science, Chulalongkorn University

Email Address: <u>Teerapong.B@Chula.ac.th</u>

Project Period: 3 years

Transcriptome profiling of the 'KDML105' rice and its transgenic derivative over-expressing OsCaM1-1 has revealed 1,756 and 1,190 genes with significantly different expression levels when grown under normal and salt stress conditions, respectively. Gene Ontology (GO) Enrichment analysis of differentially expressed genes under salt stress with higher expression level in the transgenic rice showed that GO terms involved with carbohydrate metabolic process, protein phosphorylation, response to water, regulation of transcription, and lipid transport were enriched. Expression of differentially expressed genes was verified by real-time RT-PCR including those encoding a transcription factor AP2, β -amylase, isocitrate lyase, malate synthase, aconitase, ERD1, and glycosyl hydrolase. Pathway analysis by Mapman revealed that genes with higher expression levels in the transgenic rice were mapped to cellular processes including transcription, starch and sucrose degradation, and glycolysis, tricarboxylic acid cycle and glyoxylate cycle suggesting that OsCan1-1 overexpression may affect carbohydrate metabolism in rice grown under salt stress. Expression of OsICL, which encodes isocitrate lyase was confirmed to be higher in all three available transgenic rice lines when grown in both normal and salt stress conditions presenting a good candidate for further characterization.

Previously, putative OsCaM1 and OsCML3 target putative proteins were identified from rice by cDNA expression library screening. One of the putative OsCaM1 target protein is Myosin heavy chain like (MHCL) protein. Here, the pull-down assay showed that OsCaM1 interacted with OsMHCL in the presence of calcium. In addition, the yeast two-hybrid system showed that OsMHCL interacted with OsCML4, OsCMK5, and OsCML8 both in the presence and in the absence of calcium. For the characterization of the CaM-like protein, OsCML3 and its truncated form lacking the C-terminal extension (OsCML3m), they were found to exhibit a Ca²⁺-binding property and subsequent conformational change, but the ability to bind the CaM kinase II peptide was only observed for OsCML3m. Changes in their secondary structure upon Ca²⁺-binding measured by CD revealed that OsCML3m had a higher helical content than OsCML3. Moreover, OsCML3 was mainly localized at the plasma membrane, whereas OsCML3m was found in the nucleus. The rice high mobility group B1 (OsHMGB1) protein was identified as one of the putative OsCML3 targets. Bimolecular fluorescence complementation analysis revealed that OsHMGB1 bound OsCML3, OsCML3m or OsCML3s (cysteine to serine mutation at the prenylation site) in the nucleus, confirming that OsHMGB1 is a target protein in planta. Examination of the effect of OsCML3 or OsCML3m on the DNA-binding ability of OsHMGB1 revealed that OsCML3m decreased the level of OsHMGB1 binding to pUC19 double stranded DNA whereas OsCML3 did not. Taken together, OsCML3 probably provides a mechanism for manipulating the DNA-binding ability of OsHMGB1 in the nucleus and its C-terminal extension provides a regulatory switch.

Keywords: calmodulin; CaM; transcriptome; rice

Introduction

To tolerate salt stress, plants have evolutionarily developed several mechanisms. Some have special anatomical and morphological adaptations, others have highly-regulated physiologically adaptive mechanisms such as the compartmentalization of the cytotoxic ions, typically Na⁺ and Cl⁻, into the vacuole. However, the proceeding events, which involve how plants perceive and transduce the initial signals to elicit the appropriate responses including the sequestration of the cytotoxic ions, are needed to be identified. Beside the ion cytotoxicity, salt stress also causes the primary effect, which is the water potential reduction that leads to cellular dehydration. Both of these primary effects also lead to several secondary effects that plants have to cope with, such as reduced cellular and metabolic activities, photosynthesis inhibition, ROS production, and cell death. Therefore, under saline environments, in addition to coping with the ion cytotoxicity, plants must perceive and transduce the hyperosmotic stress, as well as minimize the secondary effects that may occur.

Since calmodulin, a multifunctional protein, likely represents one of the important nodes, which can be considered a major hub for transducing Ca²⁺ signals, which are generated by many developmental events and numerous stimuli including salt stress. Altering expression of calmodulin gene would likely affect several nodes within the signal transduction and transcriptional regulation networks. In general, even though Ca²⁺ signaling and Ca²⁺/CaM regulation appear to mediate plant responses to environmental stress, the downstream effects of CaM in response to environmental stress remain largely unknown. We would like to discover the mechanisms that generate these effects, which include identifying genes, proteins, pathways and cellular processes that are regulated by this early Ca²⁺-controlled molecular switch.

Therefore, this work will attempt to characterize the mechanisms carried out by OsCaM1, a calmodulin protein in rice and to identify other important nodes that are connected to OsCaM1. Because CaM is a multifunctional protein that regulates activities of numerous target proteins, genome-wide analysis techniques such as transcriptome and proteome profiling are particularly suitable for identifying the effectors or cellular processes that are potentially regulated by CaM. In this project, two strategies will be used. First, gene expression profiling in a genome-wide scale will be conducted on the transgenic rice lines that over-express OsCam1-1 gene when grown under salt stress. Previously, we have generated such transgenic rice lines overexpressing OsCam1-1, which appeared more tolerant to salt stress than the control plants (Figure 1) as they exhibited better ability in maintaining the shoot and the root dry weights during salt stress (Figure 2) (Saeng-ngam et al., 2012). Therefore, OsCaM1 likely plays essential roles as the early messenger to convey the message of the Ca²⁺ signal generated by salt stress.

In this study, we used RNA-Seq, an approach to transcriptome profiling using the 2nd generation sequencing technology, Illumina Genome Analyzer platform. This approach targeted only the differences in transcripts whose expression levels were affected by the over-expression of *OsCam1-1* gene in the transgenic rice plants compared with the transgenic control plants. We discovered a list of up-regulated and down-regulated genes whose expression levels were altered by this manipulation, pointing to the cellular processes that possibly involve in the responses mediated by CaM1 under salt stress.



Figure 1 The phenotype comparison of (i) wild type (KDML-wt) rice cultivar, the three transgenic rice lines, (ii) CaM1-1T1, (iii) CaM1-1T2 and (iv) CaM1-1T3, and (v) the control KDML-vector (T1) line, all grown under (A) normal or (B) salt-stress conditions for 15 d.

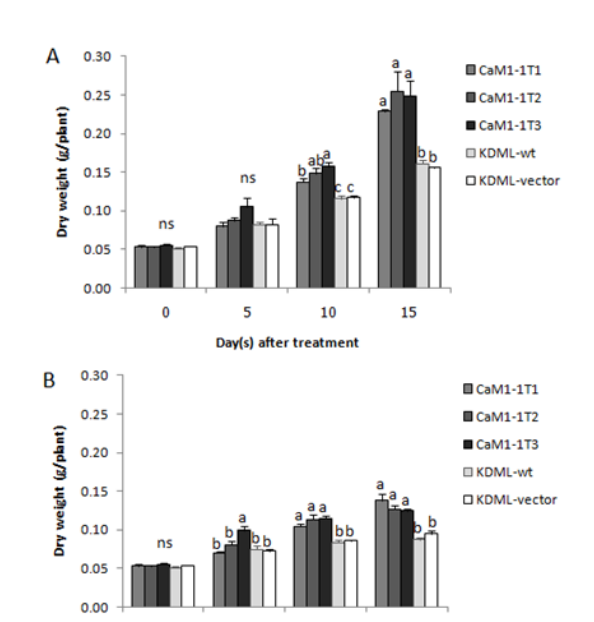


Figure 2 The dry weight of the overexpressing OsCam1-1 transgenic lines (35SCaM1-1T1, 35SCaM1-1T2 and 35SCaM1-1T3), the control transgenic line (T1; KDML-vector) and the wild type KDML105 rice cultivar, plants grown under (A) normal and (B) salt-stress conditions. Means with a different lowercase letter differ significantly (P < 0.05; DMRT), when the comparison was performed with the data at the same period of time.

Day(s) after treatment

Since Ca²⁺-mediated action of CaM depends on specific CaM-target protein interactions, meaning that CaM does not possess an enzymatic activity but, in the presence of Ca²⁺, it functions by binding to and altering the activities of various proteins, therefore we have earlier identified several putative OsCaM1 target proteins by cDNA expression library screening in hope of identifying downstream elements of transduction pathways mediating responses to salt stress via CaM1. Here, putative target proteins of CaM1 as well as a CaM-like (CML) 3 were

characterized. Their identities are valuable for identifying what effectors or cellular processes CaM1 and CML3 potentially regulates and how CaM1 and CML3 acts in a molecular detail. By these studies, genes that likely represent important nodes in the signal transduction and transcription regulation networks of Ca²⁺ signals in conjunction with calmodulin and its related sensor proteins under salt stress were identified.

Materials and Methods

Preparation of plant materials and RNA isolation

The transgenic *Oryza sativa* L. cv. KDML105 rice line overexpressing *OsCam1-1* and the control rice line, which was generated similarly to the overexpressing line but without the inserted gene, were hydroponically grown in the greenhouse. Three-week old rice seedlings were treated with salt stress by transferring the seedlings to the medium containing 150 mM NaCl. For transcriptomics, the experiments were done in two replicates. For confirmation of differentially expressed genes obtained from the transcriptome analysis, the experiments were done in three replicates. After four hours, shoots were collected and immediately frozen in liquid nitrogen and stored at -80°C. Rice tissues were ground in liquid nitrogen to fine power. For isocitrate lyase (icl) gene (LOC_Os07g34520) expression analysis, the first and third/fourth leaves were separately collected. Total RNA was isolated using TRI REAGENT (Molecular Research Center) according the manufacturer's instruction. In the final step, RNA was precipitated by mixing with 0.5 ml isopropanol per 1 ml of TRI REAGENT used for the initial homogenization.

Library preparation

Library preparation consisted of the first four following steps. (1) mRNA isolation - mRNA was isolated from 10-25 μ g of total RNA using the Invitrogen Dynabeads® magnetic separation technology. (2) First strand cDNA synthesis - The Invitrogen SuperScript® III First-Strand Synthesis Kit was used to synthesize the first strand cDNA using random hexamers. The reaction was incubated in a PCR machine under the following program: 25°C for 5 min, 50°C for 60 min, and 70°C for 15 min. (3) Second strand synthesis - The second strand cDNA was synthesized in a reaction consisting of DNA polymerase I (50 Units/100 μ l) and RNaseH (1.6 Units/100 μ l) at 16°C for 2.5 hours. The cDNA product was then cleaned up using AMPure (Agencourt). (4) DNA fragmentation - The NEB dsDNA fragmentase was added to generate dsDNA breaks in a time-dependent manner. The DNA product was then cleaned up using AMPure.

Then, the next four steps include the followings. (5) End repair - The DNA ends was repaired using the NEBNext® End Repair Enzyme Mix (NEB). The reaction was then cleaned up using AMPure. (6) Addition of 'A' bases to the 3' end of the DNA fragments - 'A' nucleotides were added to the DNA ends using Klenow exo⁻ (NEB). The reaction was then be cleaned up using AMPure. (6) Ligation adapters to DNA fragments - Premixed adapters were ligated using the NEB quick ligation ligase. The ligation product was then cleaned up using AMPure. (7) Enrichment of the adapter-modified DNA fragments by PCR - The DNA was enriched by DNA polymerase using premixed adapter primers in a PCR machine under the following program:

98°C for 30 sec, 14 cycles of 98°C for 10 sec, 65°C for 30 sec and 72°C for 30 sec, then followed by 72°C for 5 min. The PCR product was then cleaned up using AMPure. The final DNA was eluted in 20 μ l EB.

Illumina sequencing

High-throughput sequencing by Illumina was conducted using the facilities at University of California at Berkeley, USA, in collaboration with Professor Luca Comai, University of California at Davis. Four-base barcoded adaptors were used, so six libraries with different barcodes can be pooled into one 50-base single-end read sequencing lane.

Bioinformatic analysis

The resulting sequence reads was aligned with the reference rice genome Release 7 at the Rice Genome Annotation Project (http://rice.plantbiology.msu.edu) (Ouyang, 2007) and RNA expression levels determined by the bioinformatic pipeline developed at the laboratory of Professor Luca Comai, University of California at Davis, USA. Mapman Application Sorfware (http://mapman.gabipd.org) (Thimm, 2004) was used to gain insights into what cellular processes that OsCaM1 potentially regulates in response to salt stress.

cDNA synthesis and real-time PCR

The first cDNA synthesis was synthesized by iScript cDNA synthesis kit (Bio-Rad) according to the manufacturer's instruction. Then, PCR was performed in a final volume of 20 μ l, which contained a 2- μ l aliquot of the first strand cDNA reaction, 0.05 mM of each of the gene-specific primers, and 1x SsoFast EvaGreen Supermix (Bio-Rad). The reaction included an initial 8 min denaturation at 95°C, followed by 40 cycles of PCR (95°C for 30 sec; Ta°C for 30 sec; 72°C for 45 sec. The specific oligonucleotide primers for each gene examined and its Ta are shown in Table 1.

The OsEF1 α (AK105030) gene was used as an internal control via the specific primers EF1alp-F1 and EF1alp-R1 (Table 1). The PCR reactions were performed as above with the annealing temperature of 57.9°C. The level of gene expression was determined in comparison with OsEF1 α gene expression with reference to the expression of the wild-type. The PCR reaction of the same cDNA preparation was performed in triplicate for technical replication.

Table 1 Oligonucleotide primer sequences used in this study.

| Gene | Primer | Sequence | T _a (°C) |
|---------------------|--|-------------------------------|------------------------|
| AP2 Forward 5 | | 5'- CTGTGGAGCTTCGACGACTT -3' | 59.6 |
| | Reverse | 5'- ACAAACACAAACACCGCAAT -3' | |
| eta-amylase | Forward | 5'- ATGGATGATGCCCCCTGT -3' | 57.0 |
| | Reverse | 5'- TTGGGGTACACGTCTCATGT -3' | |
| ERD1 | Forward | 5'- GAGCCACCTGAATGAGAAGG -3' | 59.6 |
| | Reverse | 5'- TTATATGCCCGAACGAATCC -3' | |
| glycosyl | Forward | 5'- GCTCAGGTGTGTGTGCA -3' | 59.6 |
| hydrolase | Reverse | 5'- CGACAGCACCACTCCTCTGT -3' | |
| isocitrate | isocitrate Forward 5'- AGAGCAGCCATGTTCTT -3' | | 59.6 |
| lyase | Reverse | 5'- CGTGCGTGCTGTAGTTCAGT -3' | |
| malate | Forward | 5'- CGTACAACCTCATCGTGGTG -3' | 59.6 |
| synthase | Reverse | 5'- CGGAGAAGTTACACGGAGAGA -3' | |
| aconitase | Forward | 5'- CATCCTCCCATACGTCATCC -3' | 59.6 |
| | Reverse | 5'- TGTCTCCTGCGGCTTTATTT -3' | |
| myosin | Forward | 5'- TGTACAGAAAGCTTCTGCTGG -3' | 59.0 |
| heavy chain like | Reverse | 5'- TTATACAGATTTGTCCCCAGG -3' | |
| EF1α | EF1lpha Forward 5'- ATGGTTGTGGAGACCTTC -3' | | 57.9 |
| | Reverse | 5'- TCACCTTGGCACCGGTTG -3' | |

Electrophoretic Shift Analysis

To analyze the recombinant proteins by electrophoresis shift assay, a final concentration of 1 mM $CaCl_2$ or 3 mM ethyleneglycoltetraacetic acid (EGTA) was added to each protein (500 pmole) solution, mixed and then resolved by sodium dodecylsulfate-polyacrylamide gel electropho- resis (SDS-PAGE) with a 12.5% (w/v) acrylamide resolving gel. Proteins were then detected by Coomassie blue staining. To examine their peptide-binding ability, each protein (200 pmole) was mixed with the peptide derived from CaMKII (Sigma) at different molar equivalents and then analyzed as previously described.

Circular Dichroism (CD) Spectroscopy

CD spectroscopy was performed at 25 $^{\circ}$ C in a J-715 Spectropolari- meter (Jasco, Easton, USA) with constant N₂ flushing. The far-UV CD spectrum was measured from 190 to 250 nm in 1 mM Tris-HCl (pH 7.5) and 1 mM KCl in the presence of 1 mM CaCl₂ or 1 mM EGTA. The final protein concentration was 10 mM. All measurements were performed within 30 min after sample preparation, using a 1-mm-path-length quartz cell with a 1 s response time, 50 mdeg sensitivity, 50 nm/min scan speed and a 2.0 nm spectral bandwidth. The average of three scans was taken.

Fluorescence Measurement

Measurement of the fluorescence emission spectra of 8-anilino-1-naphthalenesulphonate (ANS; Sigma, St Louis, USA) was performed on an LS55 Luminescence Spectrometer (PerkinElmer, Waltham, USA) at 25 $^{\circ}$ C. Fluorescence emission spectra were monitored with an excitation wavelength light of 370 nm and emission spectra in the range 400–650 nm were scanned. All measurements were performed using 1 mM of protein in 1 mM Tris-HCl (pH 7.5)/1 mM KCl with ANS at a final concentration of 100 mM in the presence of 1 mM CaCl₂ or 1 mM EGTA.

Screening of Rice cDNA Expression Library

The ³⁵S-labeled purified rOsCaM1, rOsCML3 and rOsCML3m proteins were prepared as probes to screen a rice cDNA expression library. To construct the library, polyadenylated RNA was purified from the 'KDML105' rice total RNA using the GenElute mRNA Miniprep Kit (Sigma, USA) and then used as template for cDNA synthesis using the cDNA synthesis Kit (Stratagene, USA). The Uni-ZAP XR Vector Kit (Stratagene, USA) was used to ligate the prepared rice cDNA to the lambda vector, resulting in the primary library. Primary, secondary and tertiary screenings of the amplified library were performed. Single clones were excised and analyzed with the *Pst*I restriction enzyme. All unique pBluescript SK(+) plasmids obtained from the single-clone excision were sequenced. The obtained sequences were BLAST-searched against the Rice Genome Annotation Project and Rice Annotation Project databases to identify the cloned cDNA inserts.

Pull down assay

The *E. coli* plasmid expressing *MHCL* gene was constructed by cloning the *MHCL* cDNA clone into the expression vector pRZ850 using the forward primer: 5'-ATGCGGATCCGTCAAAGCTGCAGTAAGCTTA-3' and the reverse primer: 5'-ATGCGCGGCCGCTAACTCTTTCTGGGCCAA GTG-3', respectively. The recombinant MHCL protein

was expressed in *E. coli* strain NiCo21(DE3). The His-tagged MHCL protein was purified by gravity-flow Ni-NTA agarose chromatography. Calmodulin Sepharose 4B, calmodulin immobilized by the CNBr method to Sepharose 4B, was used for testing of the interaction of the MHCL with the calmodulin. To verify the interaction, protein blot analysis on the PVDF membrane was performed using Biotinylated AtCaM2 with Streptavidin-HRP.

Yeast two hybrid analysis

The coding regions of *OsCaM, OsCML* and *MHCL* genes were amplified from their respective cDNA clones, which were obtained from the National Institute of Agrobiological Sciences, Japan. The forward and reverse primers of each gene were designed based on the cDNA sequences from the database. The sequence and the length of the oligonucleotide primers are shown in Table 2. PCR products were cloned into pENTRTM/D-TOPO and subsequently cloned into either pDESTTM32 or pDESTTM22 to generate bait and prey plasmids by LR recombination. For testing of the activation of *HIS3* reporter gene, serial dilution of MaV203 yeast cells transformed with a selected pair of resulting plasmids were dropped on the SC-LTH +3AT medium plates. The bait auto-activation was performed by transforming the *gene*-pDESTTM32 and the empty vector pDESTTM22 into yeast strain MaV203. Serial dilutions of the transformed yeast cells were dropped on the SC-LTH +3AT plates containing either CaCl₂ or EGTA.

Subcellular Localization

To construct the pCAMBIA1302 containing either *OsCML3m* fused with *GFP* at the N-terminal end, the coding region of *OsCML3*, *OsCML3m* and *GFP* were PCR amplified using the primers shown in Table 1. All PCR reactions were performed using *Ven*t DNA polymerase (NEB, Ipswich, USA) with 30 cycles of 94 °C for 1 min, 59.3 °C for 1 min and 72 °C for 1 min and 30 s and then followed by a final 72 °C for 10 min. The resulting amplicons were cloned into the T&A cloning vector (RBC, Taiwan) to give pTA-OsCML3, pTA-OsCML3m and pTA-OsGFP, respectively. The gene fragments of *OsCML3* and *OsCML3m* were individually inserted into pTA-OsGFP via the *Xho* I and *Bst*E II sites at the 3' end of the GFP coding sequence, resulting in pTA-GFP-OsCML3 and pTA-GFP-OsCML3m, respectively. The fragments of GFP-OsCML3 and GFP-OsCML3 and pCAMBIA1302 using *Nco*I and *Bst*EII sites, resulting in pCAMBIA-GFP-OsCML3 and pCAMBIA-GFP-OsCML3m, respectively. The pCAMBIA1302 plasmids containing GFP-OsCML1 or GFP-OsCML1m were also constructed and used for comparison. Each recombinant plasmid was introduced into *Agrobacterium tumefaciens* strain GV3101 by heat shock. The solution of *Agrobacterium* was then infiltrated into the leaf of tobacco plants and the plants were grown in the dark for 16 h followed by 48 h in the growth chamber. Confocal

microscopy was performed with a Leica SPE microscope (Leica, Germany) using an excitation wavelength of 488 nm.

Table 2 Oligonucleotide primers used in the yeast two-hybrid system experiment.

| Gene | Primer | Sequence (5'→3') | T _a (°C) |
|--|---|--------------------------------------|---------------------|
| OsCam1-1 | Forward | 5'-CACCATGGCGGACCAGCTCACC-3' | 58 |
| | Reverse | 5'-TCACTTGGCCATCATGACCTTG-3' | |
| OsCam2 | Forward | 5'-CACCATGGCGGACCAGCTCACC-3' | 55 |
| | Reverse | 5'-TCACTTGGCCATCATGACCTTA-3' | |
| OsCam3 | Forward | 5'-CACCATGGCGGACCAGCTCACC-3' | 57 |
| | Reverse | 5'-TTACTTGGCCATCATGACTTTAACG-3' | |
| OsCML1 | Forward | 5'-CACCATGGCGGACCAGCTCTCC-3' | 59 |
| | Reverse | 5'-TTACAGGATCACGCACTTCTGGC-3' | |
| OsCML4 | OsCML4 Forward 5'-CACCATGGAAGGGCTGACGAGC-3' | | 57 |
| | Reverse 5'-TCACCCAGATATCTTCCGTTCAG-3' | | |
| OsCML5 | Forward | Forward 5'-CACCATGGCGGAGGTGGAGGTG-3' | |
| | Reverse 5'-TTATTGGTCGGAGAGCATCATC-3' | | |
| OsCML8 | 8 Forward 5'-CACCATGGCGAGCAAATACAGAGGCT-3' | | 55 |
| Reverse 5'-CTAAAAAACCCGGCCCCA-3' | | 5'-CTAAAAAACCCGGCCCCA-3' | |
| OsCML11 | OsCML11 Forward 5'-CACCATGAGCGAGCCGGCCAC-3' | | 57 |
| Reverse 5'-TCAGGAGAAGATGTTGTCAAATGCG-3' | | | |
| OsCML13 Forward 5'-CACCATGTCTACTGTCAAGGGACAGA-3' | | 58 | |
| | Reverse 5'-CTAGTAACCATATCCAGTCCTCC-3' | | |
| OsMHCL | OsMHCL Forward 5'-CACCATGGCTACAAAACTCCGT-3' | | 53 |
| | Reverse | 5'-TTATACAGATTTGTCCCCAGG-3' | |

BiFC Assay

The gene fragments of *OsHMGB1* (AK062226), *OsCML3*, *OsCML3m* and *OsCML3s* (serine-to-cysteine mutation at the prenylation site) were amplified by PCR using individual cDNA clones from the DNA Bank of NIAS (Japan) and the respective primer pairs (Table 1). All PCR reactions were performed using KOD DNA polymerase (Toyobo, Japan) with 35 cycles of 94 °C for 1 min, 59 °C for 45 s and 68 °C for 1 min and then followed by a final 68 °C for 10 min. PCR products were ligated into the pENTR vector (Invitrogen, Japan) via a TOPO reaction, resulting in pENTR-HMGB1, pENTR-CML3, pENTR-CML3m and pENTR-CML3s, respectively. Then, the pcCFPxGW

construct [37] was used to generate pCFP-CML3, pCFP-CML3m and pCFP-CML3s by LR ClonaseTM II enzyme mix (LR recombination reactions) between pcCFPxGW and pENTR-CML3 or pENTR-CML3m or pENTR-CML3s, respectively, and prepared as above. The pnYFPxGW construct (Qu et al., 2011) was also used to construct pYFP-HMGB1 by a similar reaction between pnYFPxGW and pENTR-HMGB1. Each pair of plasmids of pCFP-CML3 and pYFP-HMGB1, or pCFP-CML3m and pYFP-HMGB1 or pCFP-CML3s and pYFP-HMGB1 was then co-transformed into Agrobacterium strain GV3101. The mixtures of the two Agrobacterium strains: GV3101 (OD₆₀₀ = 0.5) and p19 (OD₆₀₀ = 0.3) were co-infiltrated into the leaf of 6-week-old tobacco plants. The treated plants were grown in the dark for 16 h followed by 48 h in the growth chamber (Qu et al., 2011). Confocal microscopy was performed with a Fluoview FV10i (Olympus, Japan) using an excitation wavelength of 488 nm.

Electrophoretic Mobility Shift Assay (EMSA)

To generate the recombinant plasmid encoding HMGB1 fused with a (His)₆-Tag at the Nterminal end, PCR amplification by Phusion DNA polymerase (BioLab) was performed using the cDNA clone for OsHMGB1 as the template and the primer pair shown in Table 1. The PCR consisted of 30 cycles of 98 °C for 7 s, 53 °C for 20 s and 72 °C for 30 s, followed by a final 72 °C for 10 min. The PCR product was cloned into pET28b (Novagen, Darmstadt, Germany). Protein production was performed in E. coli BL21 (DE3) for 4 h by IPTG addition to a final concentration of 0.4 mM. The cells were harvested and resuspended in binding buffer I (50 mM Tris-HCl buffer pH 7.5, 30 mM imidazole, 0.5 M NaCl, 0.5 mM dithiothreitol, 1 mM EDTA and 1X protease inhibitor mix (GE Healthcare, USA)). Purification of rOsHMGB1 was performed by Nicolumn chromatography (Amersham, Little Chalfont, UK). The purified rOsHMGB1 (1.0 uM) was mixed with 100 ng pUC19 supercoiled DNA and various amounts (0-2.0 uM) of purified rOsCML3 or rOsCML3m (0–2.0 uM) in binding buffer (10 mM Tris-HCl pH 7.5, 50 mM NaCl, 1 mM DTT, 5% (v/v) glycerol, 0.05% (w/v) bromophenol blue, 0.05% (w/v) xylene cyanol) and then incubated at room temperature for 10 min. In addition, purified rOsCaM1, prepared previously [38], was incubated with rOsHMGB1 as above for direct comparison. The samples were analyzed by electrophoretic resolution in 1% (w/v) agarose-0.5x TBE, and visualized under UV-light after ethidium bromide staining, as previously described (Gresser et al., 2004).

Results and Discussion

1. Transcriptome analysis

Libraries of the *OsCam1-1*-overexpressing transgenic rice (L1) and the control wild-type rice (WT) under non-stress (NS) and stress (S) conditions were sequenced using the second-generation Illumina HiSeq2000 platform. The numbers of raw sequence reads obtained from all eight libraries are presented in Table 3. The 50-bp reads were aligned to the *Oryza sativa* japonica assembly and gene annotation Version 7 with 35,679 annotated coding genes using Bowtie (Langmead et al., 2009). The RNA-Seq data were normalized in reads per kilobase per million reads (RPKM), which considered gene length as parameter (Mortazavi et al., 2008).

Table 3 Summary of the RNA-seq libraries and their raw 50-bp sequence reads

| Plant | Condition | Abbreviation | Replicate | Raw read (Mb) |
|-----------------|-------------|--------------|-----------|------------------|
| OsCam1-1- | Non-stress | L1NS | 1 | 23.26 |
| overexpressing | | | 2 | 23.94 |
| transgenic rice | Salt stress | L1S | 1 | 22.36 |
| | | | 2 | 22.98 |
| Wild-type rice | Non-stress | WTNS | 1 | 24.02 |
| | | | 2 | 22.86 |
| | Salt stress | WTS | 1 | 23.05 |
| | | | 2 | 23.44 |

Differential expression (DESeq) analysis was carried out on the transcriptomes of the *OsCam1-1* overexpressing transgenic 'KDML' rice compared with those of the wild type 'KDML' rice when grown under normal or salt stress condition. Differentially expressed genes were identified when comparing L1NS with WTNS and comparing L1S with WTS. An overview of the number of these genes is presented in Table 4. The total number of differentially genes between L1NS vs WTNS is 1,756 and the total number of differentially expressed genes between WTNS vs WTS is 11,734 and the total number of differentially expressed genes between L1S vs WTS is 12,874.

Table 4 Number of genes differentially expressed between the *OsCam1-1*-overexpression rice and the wild-type rice

| Comparison | Number of differentially | Number of genes | Number of genes |
|--------------|--------------------------|------------------|------------------|
| | expressed genes | with higher | with higher |
| | | expression level | expression level |
| | | in WT | in L1 |
| WTNS vs L1NS | 1,756 | 956 | 800 |
| WTS vs L1S | 1190 | 338 | 852 |
| WTS vs WTNS | 11,734 | 5,997 | 5,737 |
| L1S vs L1NS | 12,874 | 5,690 | 7,184 |

All differentially expressed genes between WT and L1 were mapped onto the diagrams of metabolic pathways or other cellular processes using MapMan. Table 5 summarizes the selected genes that are differentially expressed between the OsCam1-1-overexpressing rice and the wild-type rice. Several genes obtained in Table 5 are those with higher expression level induced by salt stress (150 mM NaCl) in the OsCam1-1-overexpressing rice. This group includes genes encoding proteins or enzymes in TCA cycle (aconitate hydratase, isocitrate lyase, malate synthase), sucrose degradation (sucrose synthase, β -amylase), transcription (AP2 domain containing protein, WRKY, zinc finger protein), and several enzymes in hormone biosynthesis (NCED, GA 3- β -dioxygenase, GA 2- β -dioxygenase, oxophytodienoate reductase, lipoxygenase, allene oxide synthase, arginine decarboxylase).

One the contrary, several genes in photosynthesis pathways were found down-regulated at a higher degree in the OsCam1-1-overexpressing rice when compared with those of the control wild-type rice. They are genes encoding thylakoid lumenal protein, PSII polypeptide, PSII membrane protein, PSII reaction center subunit and chlorophyll A-B binding proteins. Expression of these genes is normally down-regulated under salt stress. However, their expression was found consistently decreased upon salt stress at a higher degree in the OsCam1-1-overexpressing rice. These genes are candidates for further investigation into the physiological functions of OsCaM1 in the Ca²⁺-mediated salt stress responses.

When pathway analysis was carried out for these genes (Figure 3), we found that they are involved in several processes including transcription (Figure 3A), starch and sucrose degradation (Figure 3B), and glycolysis, tricarboxylic acid cycle and glyoxylate cycle (Figure 3C). Several genes whose expression levels were more elevated in the transgenic rice than the wild type when grown under salt stress condition were selected for verification by real-time RT-PCR

Table 5 List of differentially expressed genes between the OsCam1-1-overexpressing rice and the control wild-type rice

| Process | Locus | Description | RPKM | | | |
|---------------|----------------|--|----------------|---------------|---------------|----------------|
| | | | WTNS | L1NS | WTS | L1S |
| TCA | LOC_Os08g09200 | Aconitate hydratase | 31.6 ± 3.6 | 30.4 ± 2.6 | 105.2 ± 5.0 | 140.0 ± 7.1 |
| | LOC_Os03g04410 | Aconitate hydratase | 18.2 ± 1.3 | 16.2 ± 0.4 | 92.1 ± 3.5 | 103.5 ± 3.5 |
| | LOC_Os07g34520 | Isocitrate lyase | 2.6 ± 0.5 | 9.6 ± 7.4 | 267.9 ± 11.1 | 458.6 ± 39.8 |
| | LOC_Os04g40990 | Malate synthase | 7.6 ± 0.5 | 13.1 ± 4.7 | 296.6 ± 36.8 | 444.9 ± 15.1 |
| Sucrose and | LOC_Os03g22120 | Sucrose synthase | 35.7 ± 8.8 | 47.6 ± 3.0 | 209.8 ± 21.6 | 262.0 ± 1.4 |
| starch | LOC_Os03g22790 | Beta-amylase | 74.3 ± 10.0 | 83.1 ± 5.7 | 215.5 ± 2.9 | 251.0 ± 16.1 |
| metabolism | LOC_Os04g45290 | Invertase | 18.6 ± 1.6 | 21.1 ± 0.4 | 21.2 ± 2.6 | 25.7 ± 1.0 |
| | LOC_Os01g22900 | Invertase | 125.8 ± 0.3 | 136.2 ± 18.6 | 94.0 ± 19.1 | 120.1 ± 15.7 |
| | LOC_Os09g08072 | Invertase | 14.6 ± 0.1 | 15.1 ± 0.8 | 23.4 ± 1.1 | 27.2 ± 4.3 |
| | LOC_Os02g33110 | Invertase | 22.3 ± 0.6 | 22.5 ± 2.4 | 6.9 ± 0.9 | 9.4 ± 0.9 |
| Transcription | LOC_Os03g08470 | AP2 domain containing protein | 8.8 ± 2.5 | 9.2 ± 1.1 | 53.9 ± 7.1 | 86.7 ± 1.0 |
| | LOC_Os04g32620 | Ethylene-responsive transcription factor | 1.3 ± 0.1 | 1.5 ± 0.2 | 7.4 ± 2.4 | 10.8 ± 1.0 |
| | LOC_Os05g41780 | AP2 domain containing protein | 33.3 ± 1.1 | 34.9 ± 6.3 | 63.1 ± 10.9 | 89.7 ± 20.5 |
| | LOC_Os08g41030 | AP2 domain containing protein | 0.0 ± 0.0 | 0.0 ± 0.0 | 2.0 ± 0.5 | 5.4 ± 0.1 |
| | LOC_Os02g08440 | WRKY71 | 15.6 ± 1.6 | 17.8 ± 6.8 | 57.9 ± 13.8 | 93.0 ± 6.4 |
| | LOC_Os03g20550 | WRKY55 | 1.9 ± 0.2 | 1.9 ± 0.0 | 13.3 ± 2.0 | 19.1 ± 0.0 |
| | LOC_Os12g39400 | C2H2 zinc finger protein | 1.6 ± 0.3 | 1.8 ± 0.1 | 16.0 ± 0.4 | 20.7 ± 0.1 |
| | LOC_Os01g55340 | C2C2-Dof zinc finger protein | 1.3 ± 0.2 | 1.4 ± 0.1 | 12.8 ± 0.4 | 19.9 ± 2.2 |
| ABA | LOC_Os07g05940 | 9-cis-epoxycarotenoid dioxygenase 1 | 2.7 ± 0.2 | 4.2 ±3.7 | 39.9 ± 17.0 | 74.2 ± 10.9 |
| metabolism | | | | | | |

| Process | Locus | Description | RPKM | | | |
|---------------------|----------------|-----------------------------------|----------------|----------------|---------------|---------------|
| | | | WTNS | L1NS | WTS | L1S |
| GA metabolism | LOC_Os01g08220 | Gibberellin 3-beta dioxygenase | 3.6 ± 1.2 | 6.0 ± 0.2 | 4.6 ± 1.1 | 7.2 ± 2.3 |
| | LOC_Os05g48700 | Gibberellin 2-beta dioxygenase | 1.0 ± 0.4 | 4.7 ± 0.6 | 27.6 ± 0.6 | 45.3 ± 6.5 |
| JA metabolism | LOC_Os01g27230 | 12-oxophytodienoate reductase | 11.7 ± 2.2 | 16.8 ± 3.1 | 10.2 ± 0.5 | 13.8 ± 2.4 |
| | LOC_Os03g49380 | Lipoxygenase | 3.2 ± 0.3 | 3.7 ± 0.2 | 20.9 ± 2.0 | 44.4 ± 8.4 |
| | LOC_Os12g37260 | Lipoxygenase | 77.8 ± 16.9 | 52.7 ± 6.5 | 23.5 ± 4.6 | 9.7 ± 3.5 |
| | LOC_Os02g12680 | Allene oxide synthase | 0.14 ± 0.07 | 0.18 ± 0.06 | 33.9 ± 8.7 | 59.8 ± 5.0 |
| Polyamine synthesis | LOC_Os06g04070 | Arginine decaboxylase | 23.1 ± 0.9 | 19.3 ± 6.0 | 20.6 ± 0.6 | 27.8 ± 4.3 |
| Photosynthesis | LOC_Os12g19470 | RUBISCO | 575.1 ± 214.3 | 552.2 ± 149.6 | 70.7 ± 8.3 | 47.2 ±7.0 |
| | LOC_Os04g59440 | Chlorophyll A-B binding protein | 30.3 ± 8.7 | 20.3 ± 9.7 | 92.8 ± 14.4 | 57.2 ± 3.2 |
| | LOC_Os01g64960 | Chlorophyll A-B binding protein | 234.5 ± 68.0 | 207.2 ± 51.6 | 28.7 ± 1.3 | 19.6 ± 2.6 |
| | LOC_Os08g39430 | thylakoid luminal 19 kDa protein | 68.5 ± 9.1 | 62.9 ± 3.8 | 22.4 ± 3.8 | 14.3 ± 3.3 |
| | LOC_Os07g05360 | Photosystem II 10 kDa polypeptide | 2071.6 ± 407.6 | 2195.2 ± 101.1 | 798.6 ± 15.6 | 582.7 ± 80.4 |
| | LOC_Os04g33830 | membrane protein | 2799.4 ± 35.7 | 2908.4 ± 73.3 | 1179.9 ± 30.6 | 877.2 ± 136.8 |
| | LOC_Os07g05480 | PSI reaction center subunit | 2502.6 ± 187.2 | 2420.9 ± 132.7 | 1185.5 ± 5.9 | 885.9 ± 68.9 |
| | LOC_Os07g25430 | PSI reaction center subunit | 2464.9 ± 243.4 | 2409.8 ± 177.6 | 913.5 ± 50.0 | 706.2 ± 58.4 |
| | LOC_Os12g08770 | PSI reaction center subunit | 1291.8 ± 159.0 | 1291.6 ± 112.2 | 417.7 ± 3.8 | 328.2 ± 50.2 |
| | LOC_Os01g41710 | Chlorophyll A-B binding protein | 7527.0 ± 159.2 | 7525.3 ± 181.1 | 1140.0 ± 36.2 | 826.1 ± 124.8 |
| | LOC_Os03g39610 | Chlorophyll A-B binding protein | 3468.4 ± 320.0 | 3310.1 ± 169.5 | 822.3 ± 14.8 | 602.8 ± 89.8 |
| | LOC_Os04g38410 | Chlorophyll A-B binding protein | 1830.6 ± 117.2 | 1688.7 ± 23.4 | 258.8 ± 22.3 | 184.2 ± 46.4 |
| | LOC_Os11g13890 | Chlorophyll A-B binding protein | 3878.4 ± 308.2 | 3819.6 ± 91.7 | 879.3 ± 85.5 | 665.9 ± 93.5 |

A.



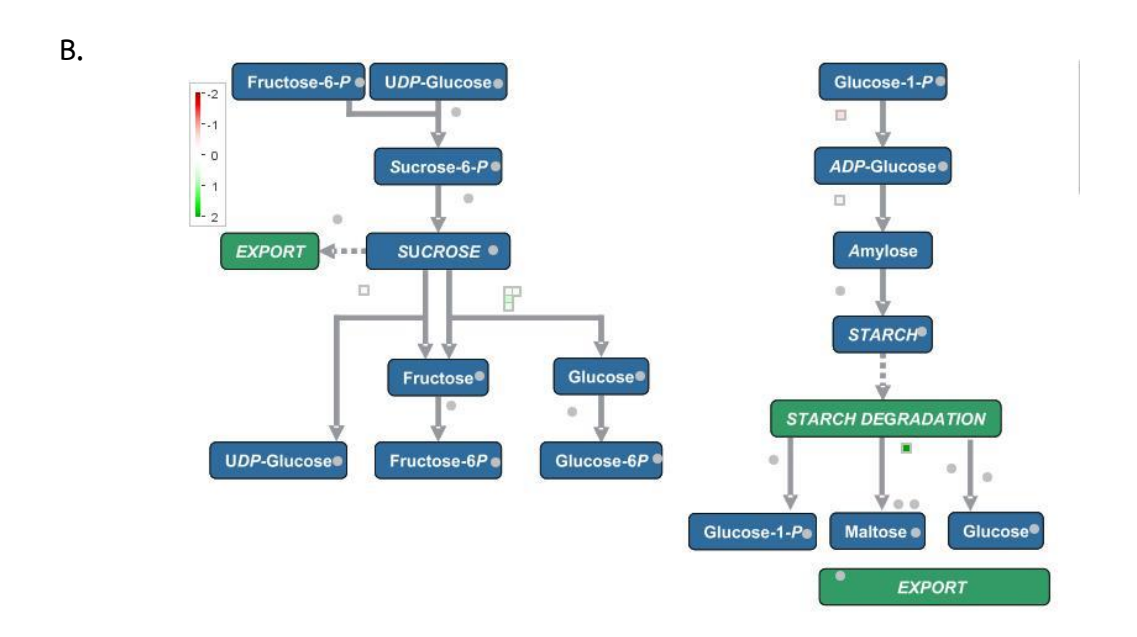


Figure 3 Mapman analysis of genes with differentially expressed levels between the wild-type and the *OsCam1-1* overexpressing transgenic rice grown under normal or salt stress condition.

A. Transcription B. sucrose-starch metabolism and C. glycolysis-TCA pathways

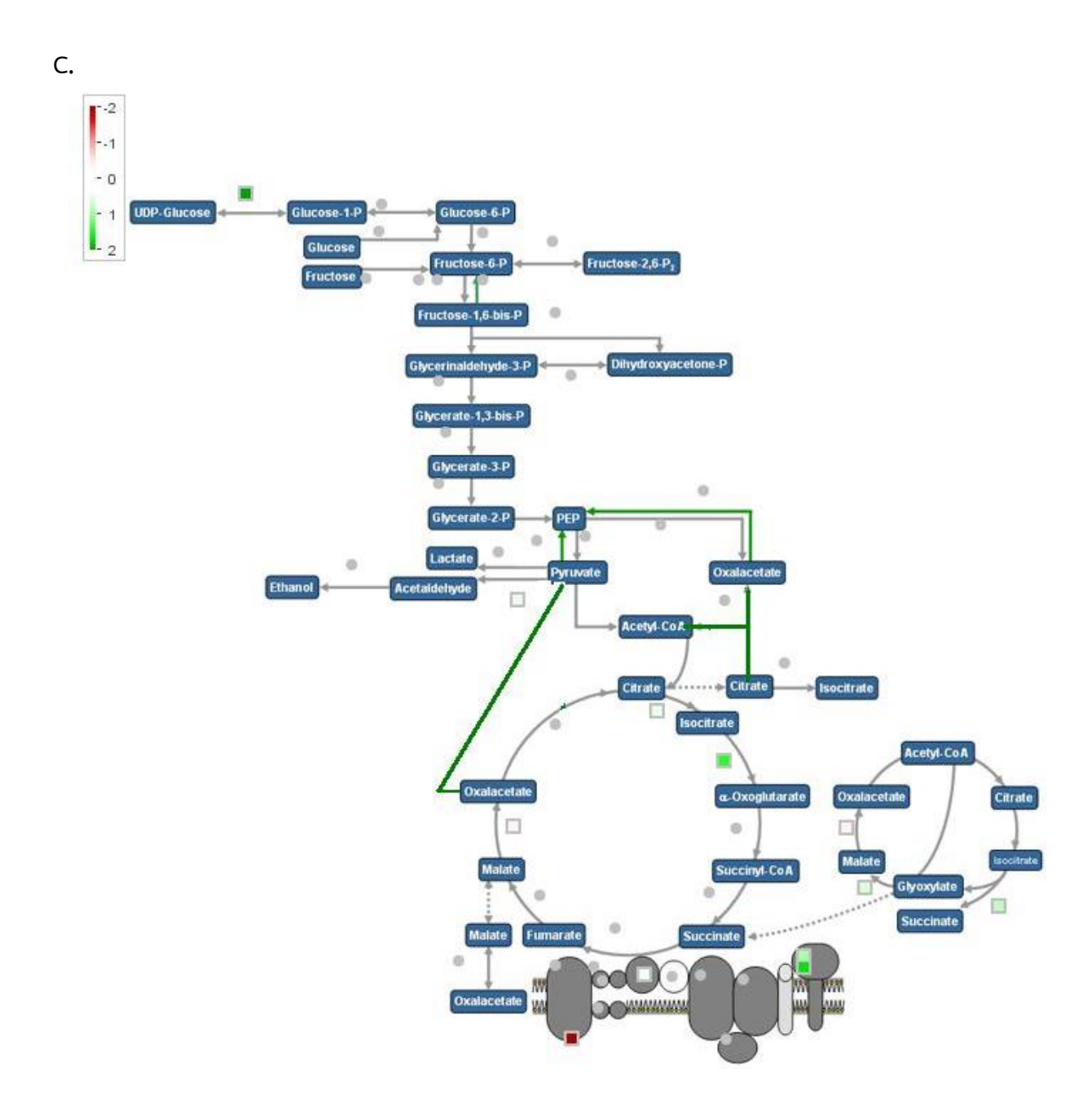


Figure 3 (Continued) Mapman analysis of genes with differentially expressed levels between the wild-type and the *OsCam1-1* overexpressing transgenic rice grown under normal or salt stress condition. A. Transcription B. sucrose-starch metabolism and C. glycolysis-TCA pathways

To show possible relations between these sets of comparison, Venn diagrams showing numbers of genes with higher or lower expression level in the transgenic rice under both normal and salt stress condition shared by differentially expressed genes under salt stress in both wild type and transgenic rice were constructed as shown in Figure 4.

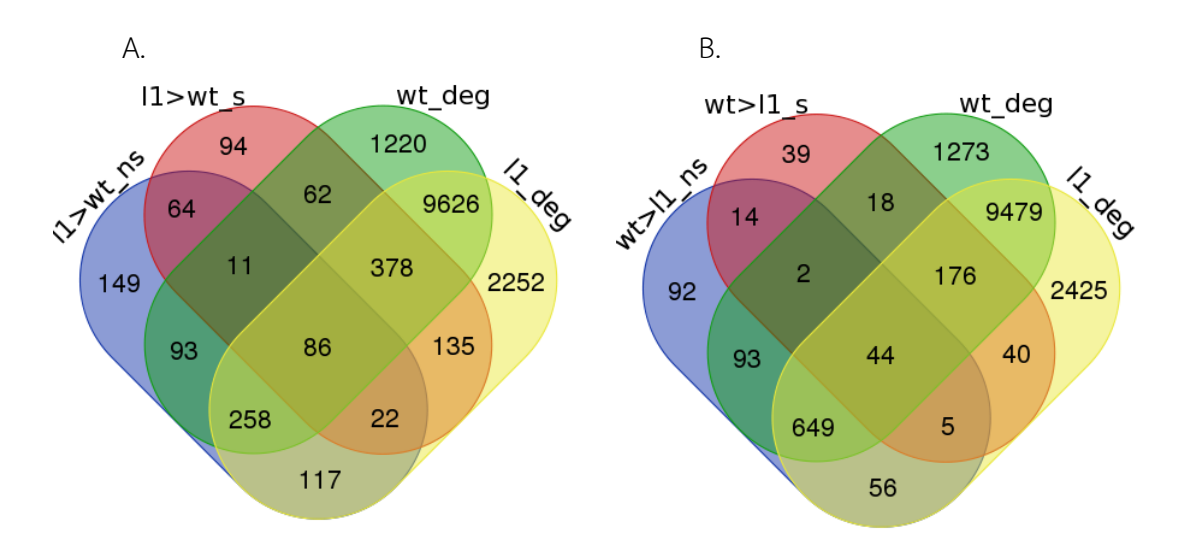


Figure 4 Venn diagrams showing numbers of differentially expressed genes under salt stress in wild type (wt_deg) and transgenic rice (l1_deg) shared by (A) genes with higher expression level in the transgenic rice under normal (l1>wt_ns) and salt stress (l1>wt_s) or (B) genes with lower expression level in the transgenic rice under normal (wt>l1_ns) and salt stress (wt>l1_s).

Analysis of differentially expressed genes under salt stress with higher expression level in the transgenic rice (Figure 4A) using Gene Ontology Enrichment analysis, in the term of biological process (Figure 5A), showed that many genes involved with carbohydrate metabolic process, protein phosphorylation, response to water, regulation of transcription, and lipid transport were enriched. In the term of molecular function (Figure 5B), enriched GO terms include sequence-specific DNA binding, heme binding, hydrolase activity, acting on glycosyl bonds, transcription activity, carbohydrate binding, protein kinases activity, electron carrier activity, and oxidoreductase activity.

Analysis of differentially expressed genes under salt stress with lower expression level in the transgenic rice (Figure 4B) using Gene Ontology Enrichment analysis, in the term of biological process (Figure 6A), showed that many genes involved with fatty acid biosynthesis process, lipid transport, amino acid metabolic process, cellulose biosynthetic process, nitrogen compound metabolic process, response to oxidative stress, translation, and

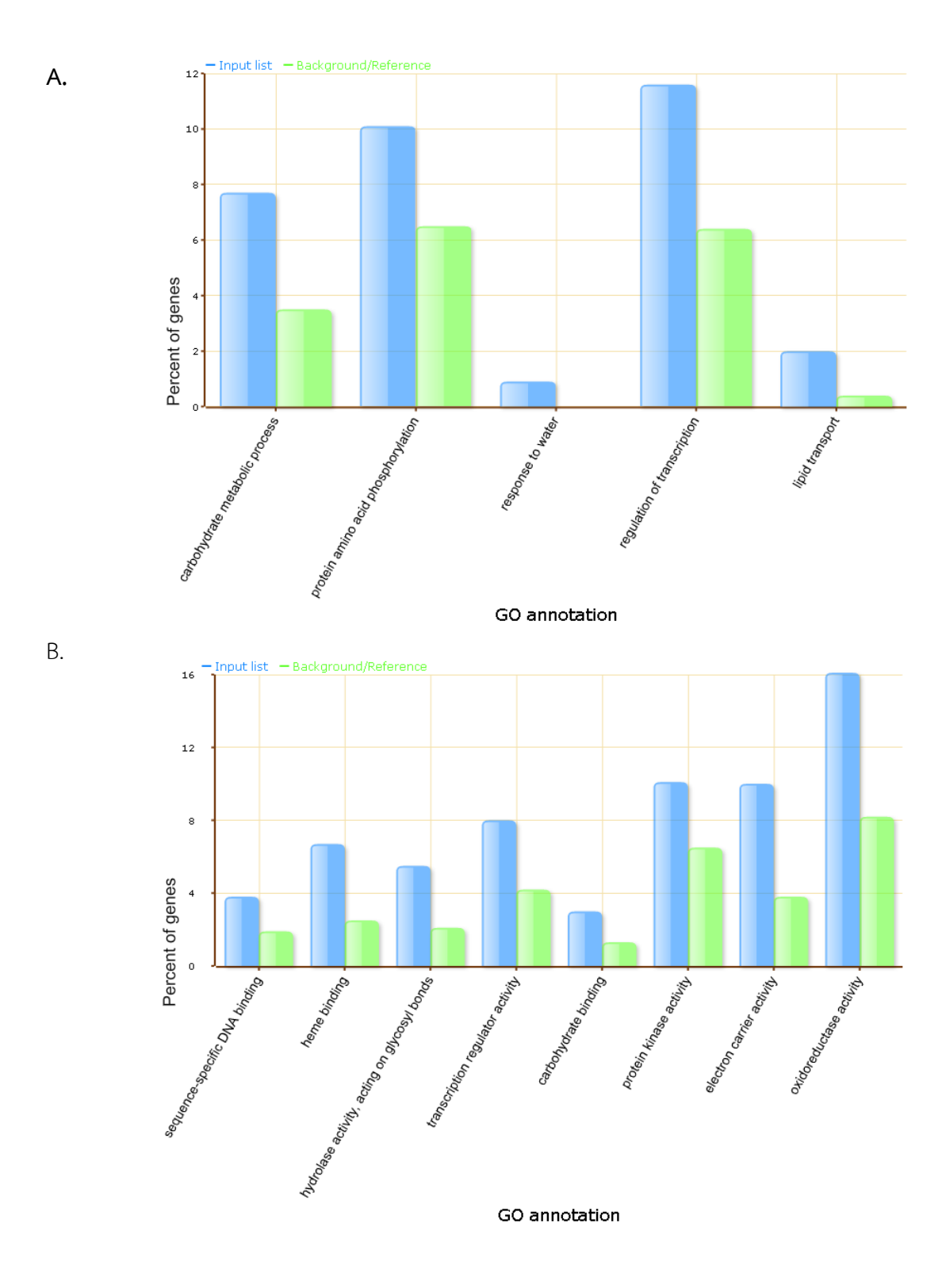


Figure 5 Gene Ontology Enrichment Analysis of differentially expressed genes under salt stress with higher expression level in the transgenic rice in term of Biological Process (A) and Molecular Function (B).

photosynthesis were enriched. In the term of molecular function, enriched GO terms include structural components of ribosome, cellulose synthase activity, and peroxidase activity (Figure 6B). Enriched GO terms in cellular component include membrane part, ribosome, and photosystem (Figure 6C).

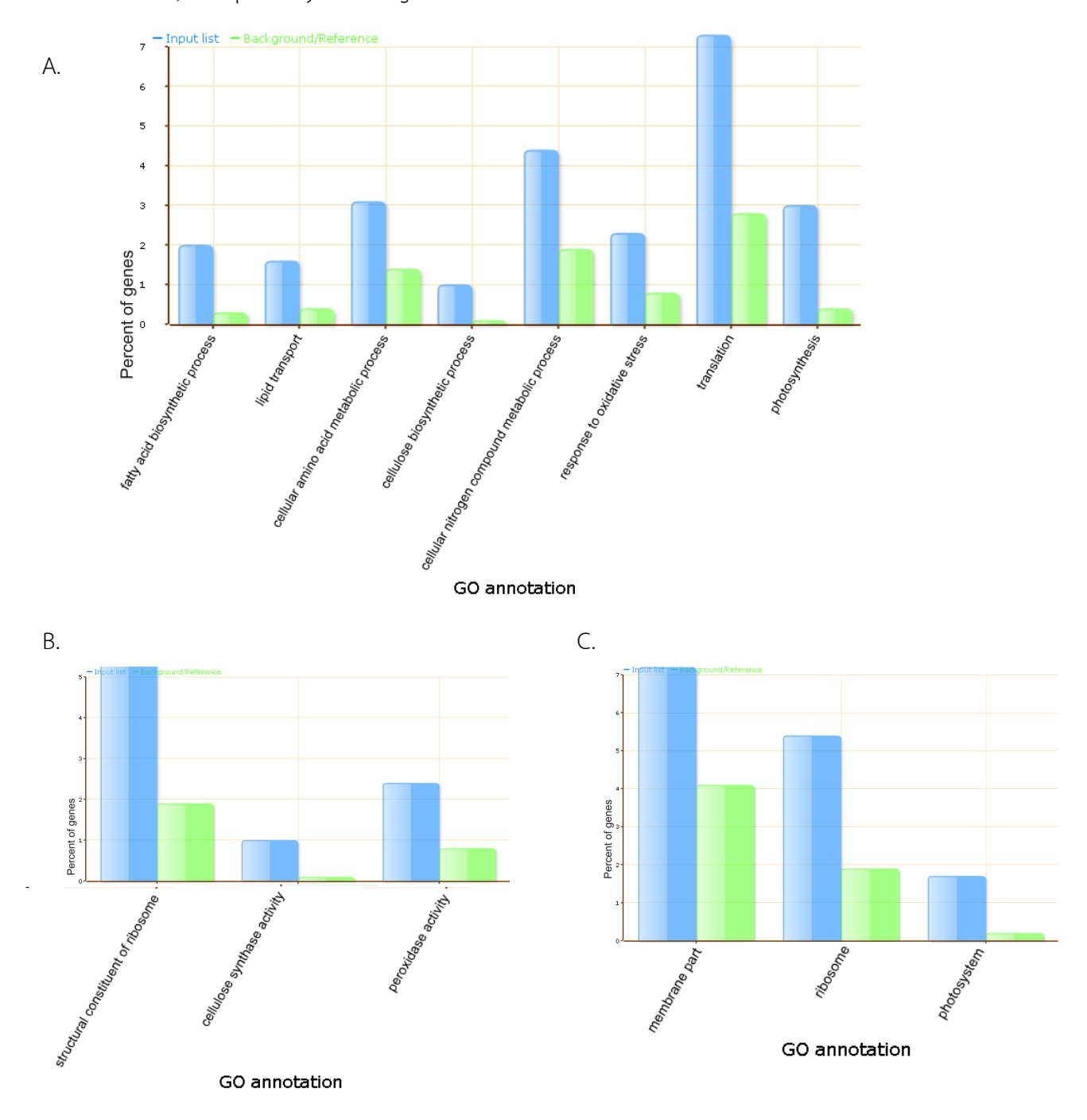


Figure 6 Gene Ontology Enrichment Analysis of differentially expressed genes under salt stress with lower expression level in the transgenic rice in term of Biological Process (A), Molecular Function (B), and Cellular Component (C).

2. Confirmation of differentially expressed genes

Real-time RT-PCR was performed to confirm the RNA-Seq result and most real-time RT-PCR results agreed well with the RNA-Seq including the genes encoding a transcription factor AP2, β -amylase, isocitrate lyase, malate synthase, aconitase, ERD1, and glycosyl hydrolase (Figure 7). In the 'KDML' rice, salt stress was found to induce the expression of these genes. Interestingly, in the transgenic rice, their expression levels were significantly higher than the wild type when grown under salt stress conditions.

Overall, the transcriptome profile showed that several genes in the core metabolism of carbohydrate were altered when *Oscam1-1* was over-expressed under salt stress suggesting that *OsCam1-1* possibly enhances the salt-tolerant ability in rice via regulating the carbohydrate metabolism.

Expression of *isocitrate lyase (icl)* gene ($LOC_Os07g34520$) was further confirmed in all three OsCam1-1 overexpressing independent transgenic lines L1, L2, and L3 that we have previously produced. The results of real-time RT-PCR are presented in graphs shown in Figure 2. In addition, expression of *icl* gene was examined in the first and third/fourth leaves of the wildtype, the control transgenic rice line, and the OsCam1-1 overexpressing Oryza sativa L. cv. KDML105 independent transgenic lines L1, L2, and L3 grown under either normal or salt stress condition. The level of gene expression was determined in comparison with $OsEF1\alpha$ gene expression with reference to the expression of the wild-type grown under normal condition. The results of real-time RT-PCR are presented in graphs shown in Figure 8 and 9.

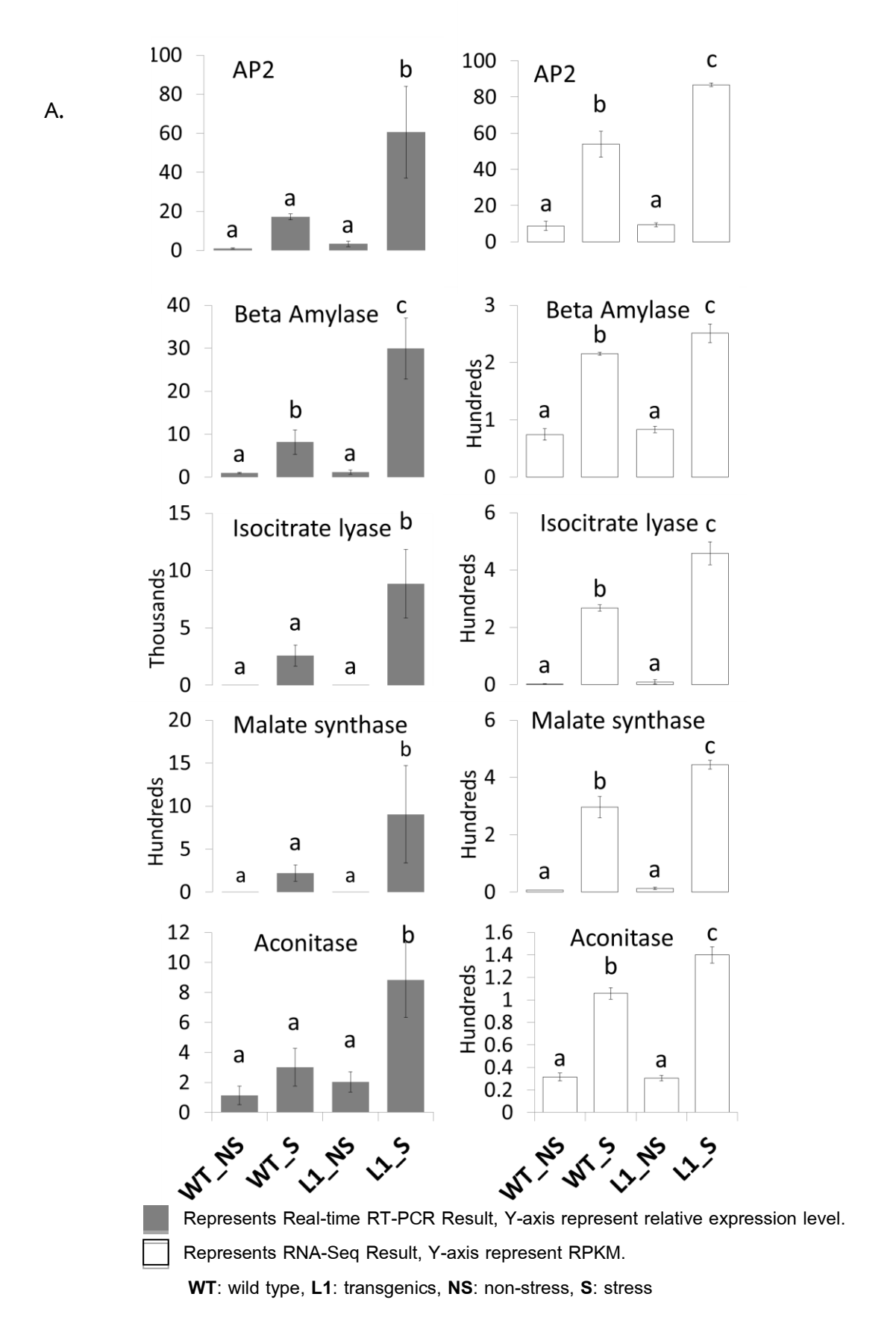


Figure 7 Expression of the selected genes differentially expressed in the *OsCam1-1* overexpressing transgenic rice compared with the wild-type rice by real-time RT-PCR.

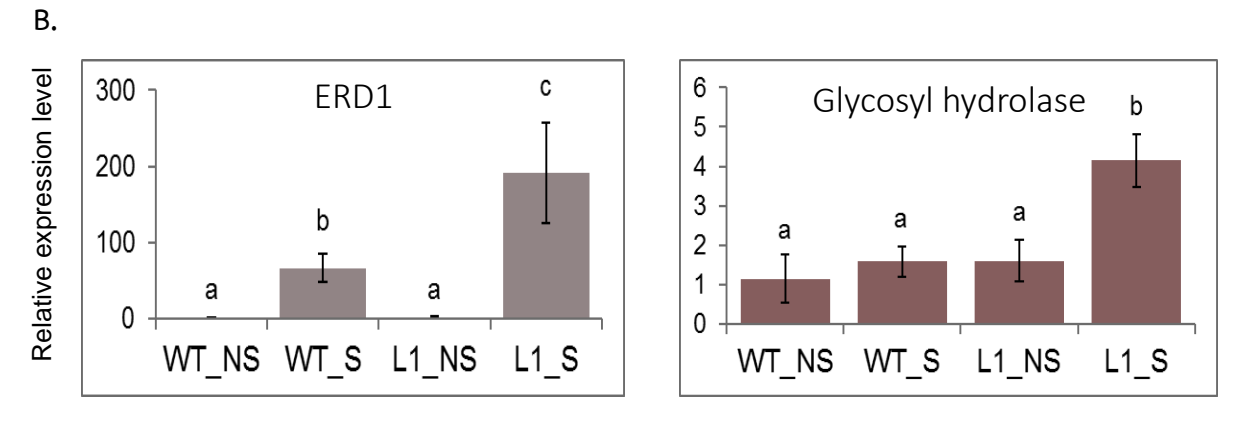
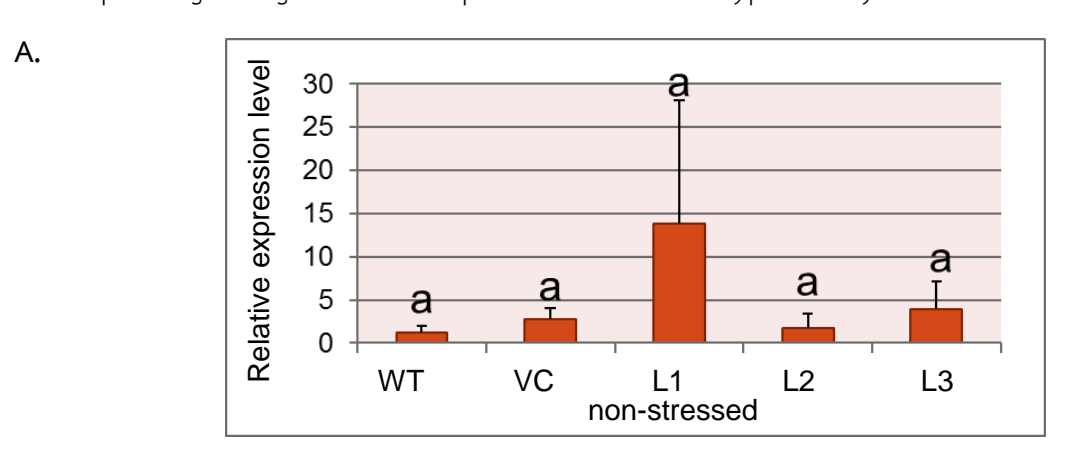


Figure 7 (Continued) Expression of the selected genes differentially expressed in the *OsCam1-1* overexpressing transgenic rice compared with the wild-type rice by real-time RT-PCR.



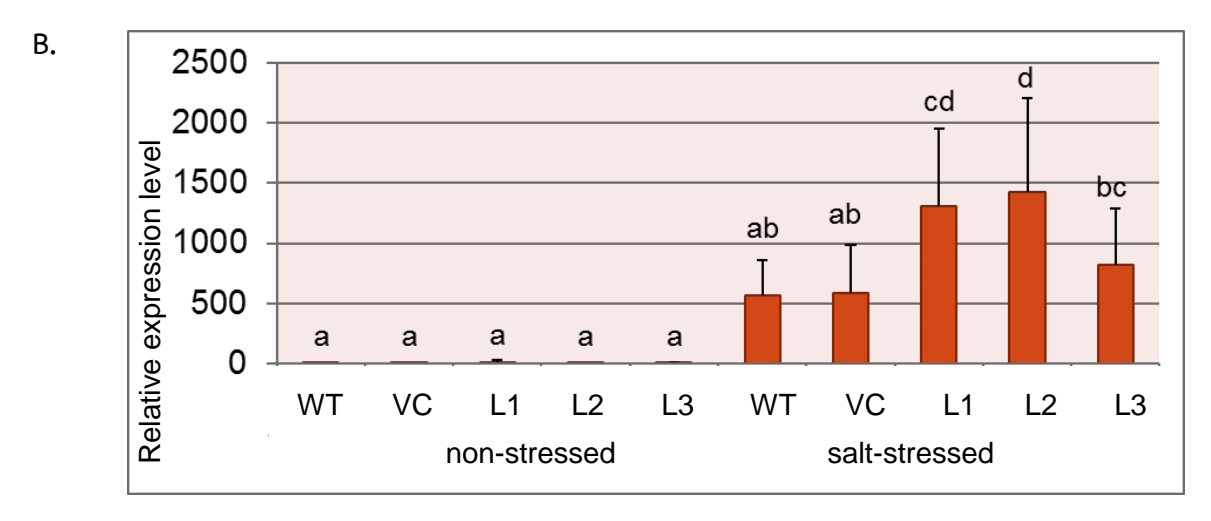
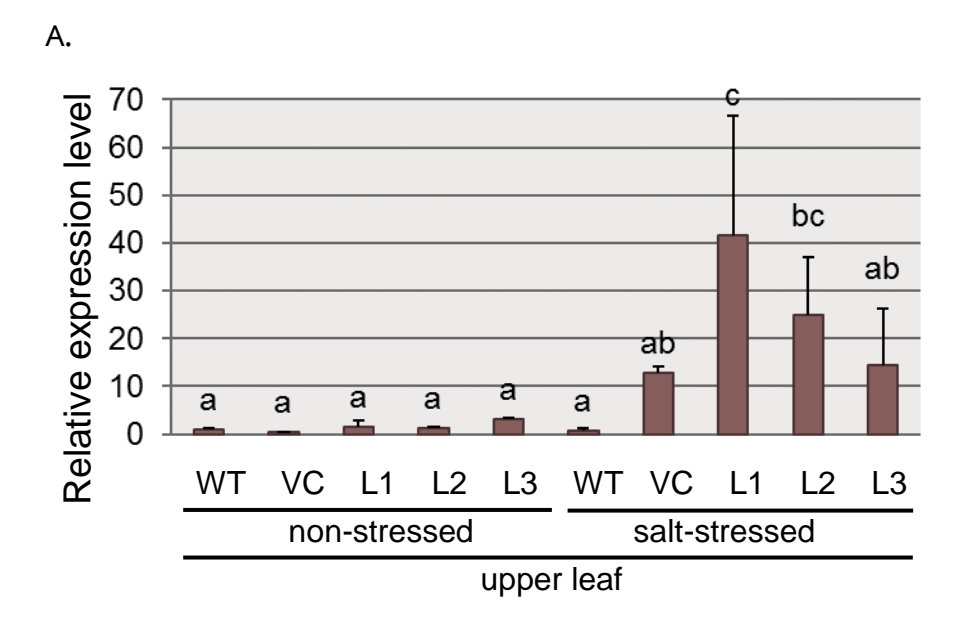


Figure 8 Expression of *isocitrate lyase* gene ($LOC_Os07g34520$) in the OsCam1-1 overexpressing transgenic rice (L1, L2, L3) compared with the wild-type rice (WT) and the control transgenic line (VC) by real-time RT-PCR either under normal (A. and B.) or salt stress (B) condition. The levels of gene expression were determined in comparison with OsEF1 α gene expression in reference with the expression of the wild-type grown under normal condition.



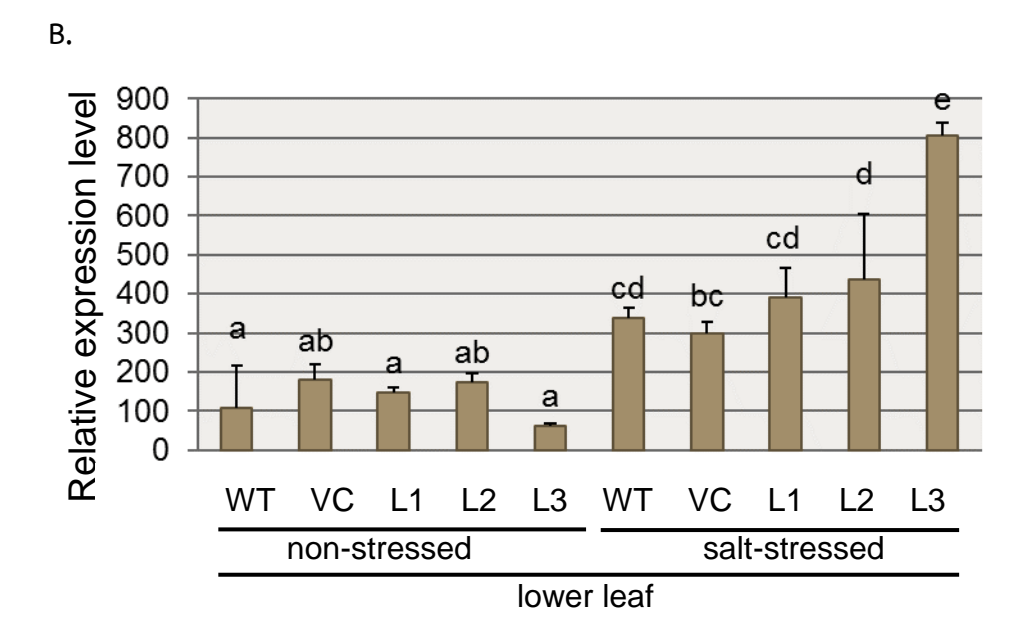


Figure 9 Expression of *isocitrate lyase* gene ($LOC_Os07g34520$) in the OsCam1-1 overexpressing transgenic rice (L1, L2, L3) compared with the wild-type rice (WT) and the control transgenic line (VC) by real-time RT-PCR of the first (A) and the third/fourth (B) leaf grown either under normal or salt stress condition. The levels of gene expression were determined in comparison with OsEF1 α gene expression in reference with the expression of the wild-type upper leaf grown under normal condition.

3. Pull down assay

The CaM binding site of *MHCL* (CBS) was searched using the Calmodulin Target Database (http://calcium.uhnres.utoronto.ca/ctdb/ctdb/). The putative CBS was cloned, expressed, and used to produce the recombinant CBS fusion protein. The binding ability of the purified recombinant protein to CaM-Sepharose was analyzed. As shown in Figure 10, the purified CBS elution 4 (Lane 8) was able to bind CaM in the presence of Ca²⁺. To confirm that the CBS fusion protein bound CaM not the resin in the column, western blot analysis was performed. The proteins from SDS-PAGE were transferred to the PVDF membrane and blotted with Biotinylated AtCaM2. The result showed that the CBS fusion protein bound AtCaM2 (Figure 11).

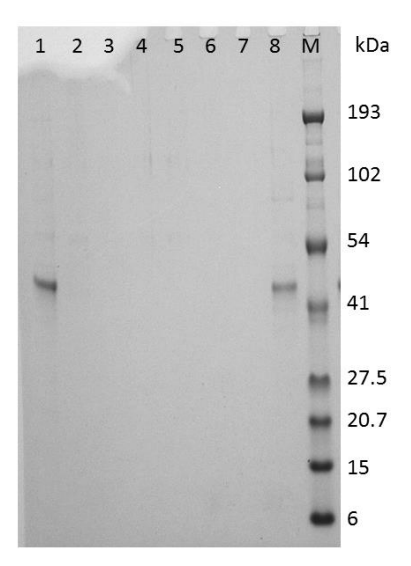


Figure 10 Analysis of the putative CaM binding domain of MHCL protein by CaM-Sepharose pull-down assay. The gel was stained with GelCode[®] Blue Stain Reagent. Lane M, prestained SDS-PAGE standards (Bio-RAD); lane 1, input protein; lane 2, unbound protein; Lane 3, wash 1; lane 4, wash 2; lane 5, purified CBS elution 1; lane 6, purified CBS elution 2; lane 7, purified CBS elution 3; lane 8, purified CBS elution 4.

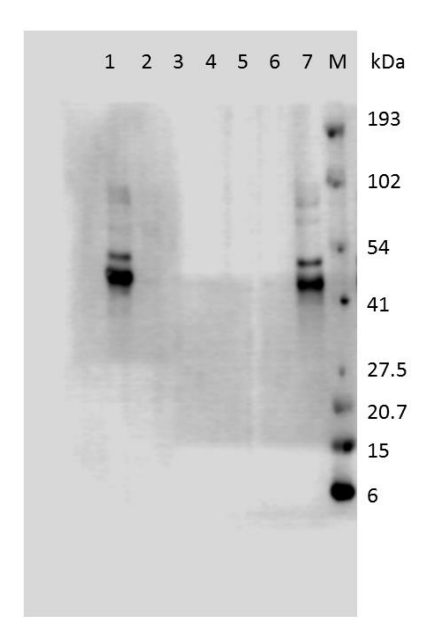


Figure 11 Western blot analysis of the CaM-Sepharose binding assay. The membrane was incubated in freshly mixed SuperSignal[®] reagents and photographed by the C-digit blot scanner. Lane M, prestained SDS-PAGE standards (Bio-RAD); lane 1, input protein; lane 2, unbound protein; lane 3, wash 2; lane 4, purified CBS elution 1; lane 5, purified CBS elution 2; lane 6 purified CBS elution 3; lane 7, purified CBS elution 4.

4. Yeast two hybrid

Interaction of the MHCL protein with OsCaM1 or other OsCaMs as well as some of the OsCML proteins was further tested using yeast two hybrid. Testing of the bait (GAL4 DBD fusion) for nonspecific activation was performed by transforming the pDESTTM32/MHCL and the empty-pDESTTM22 into the yeast strain MaV203. The extent of self-activation was accessed on the reporter gene *HIS3* by determining the concentration of *HIS3* inhibitor 3AT necessary to repress growth. This concentration would later be used in two-hybrid screening to suppress growth of yeast cells not containing interacting bait and prey. The result showed that the MHCL protein can be used as a bait protein without auto-activation of the reporter gene *HIS3* (Figure 12).

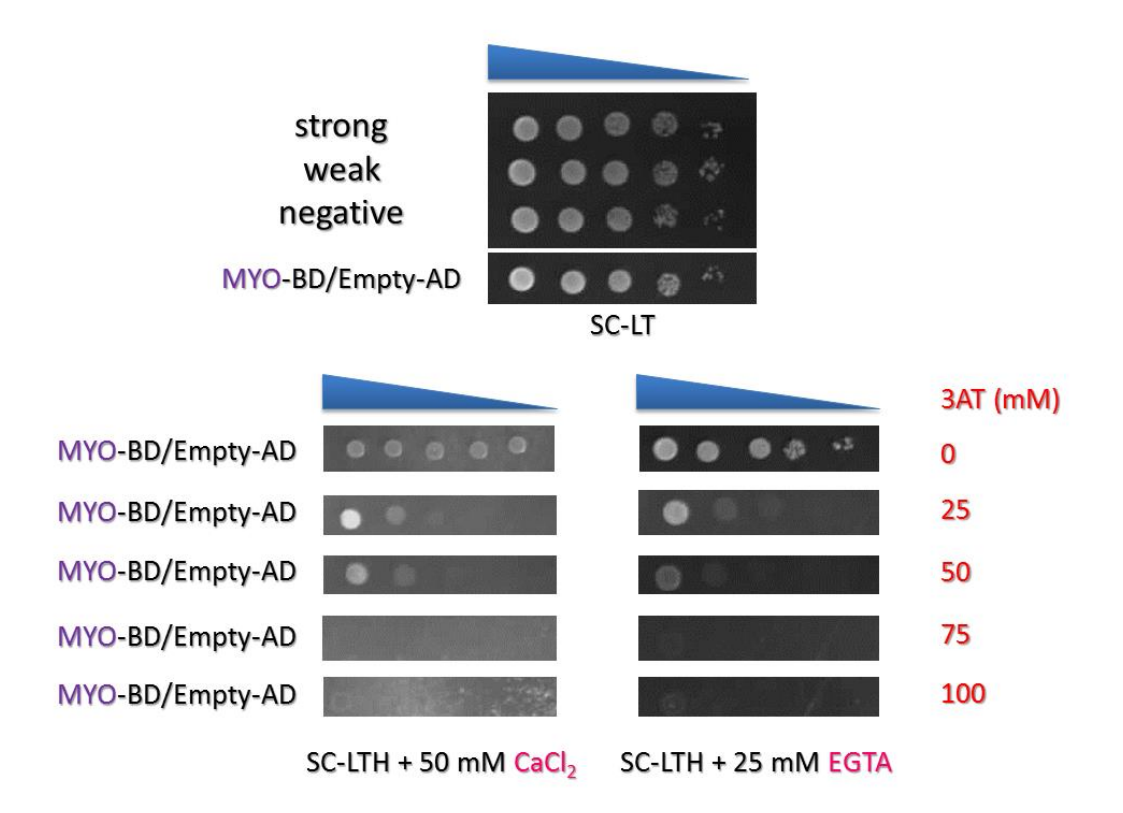


Figure 12 Testing of the bait auto-activation. Yeast strain MaV203 co-transformed with the test constructs was grown at 30 °C for several days under non-selective (SC-LT) and selective (SC-LT) conditions. Serial dilutions of transformed cells are shown by narrowing triangles.

To verify that the rice MHCL is a CaM-binding protein by yeast two hybrid, pDESTTM32/MHCL and each of the pDESTTM22 harboring OsCaM or OsCML: pDESTTM22/CaM or pDESTTM22/CML, were transformed into MaV203 cells. The result of the activation of the reporter gene *HIS3* in these transformants showed that the OsMHCL can interact with OsCML4, OsCML5 and OsCML8 proteins both in the presence and in the absence of calcium as shown in Figure 13. However, yeast two hybrid analysis did not show the interaction between OsMHCL and OsCaM1 as expected. This may be due to the flexibility of the OsCaM1 in binding with its target proteins in the cell.

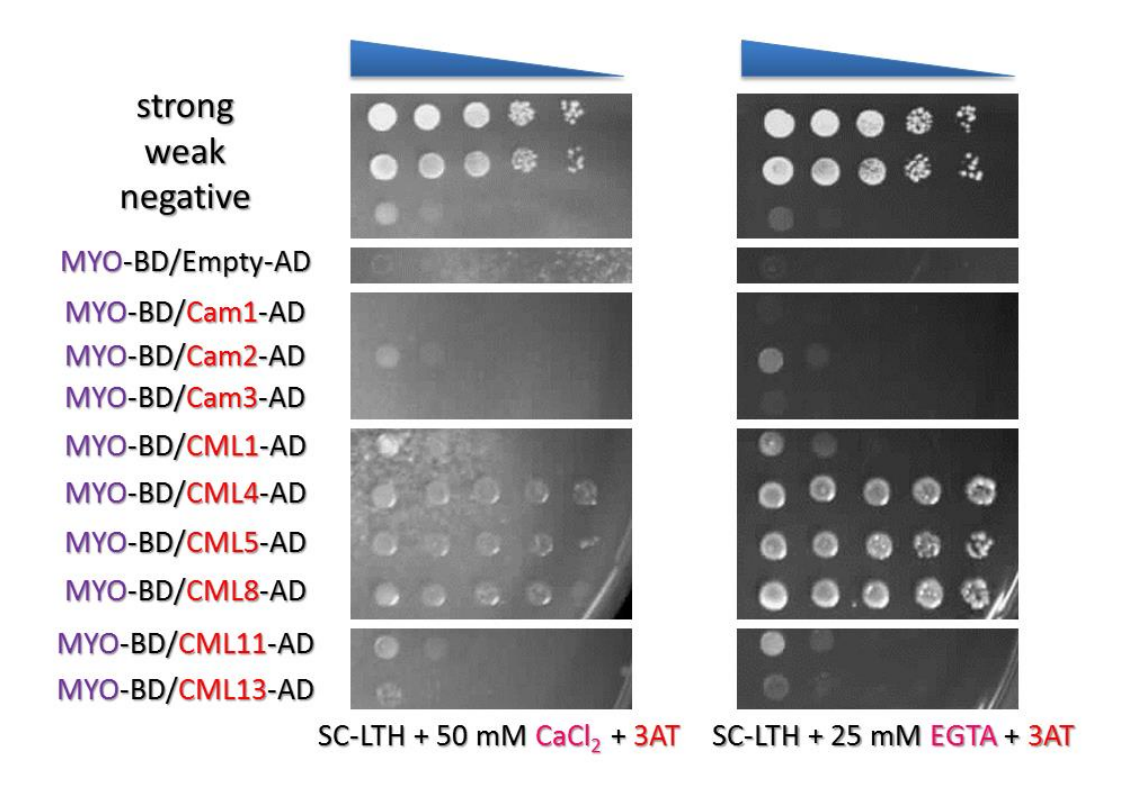
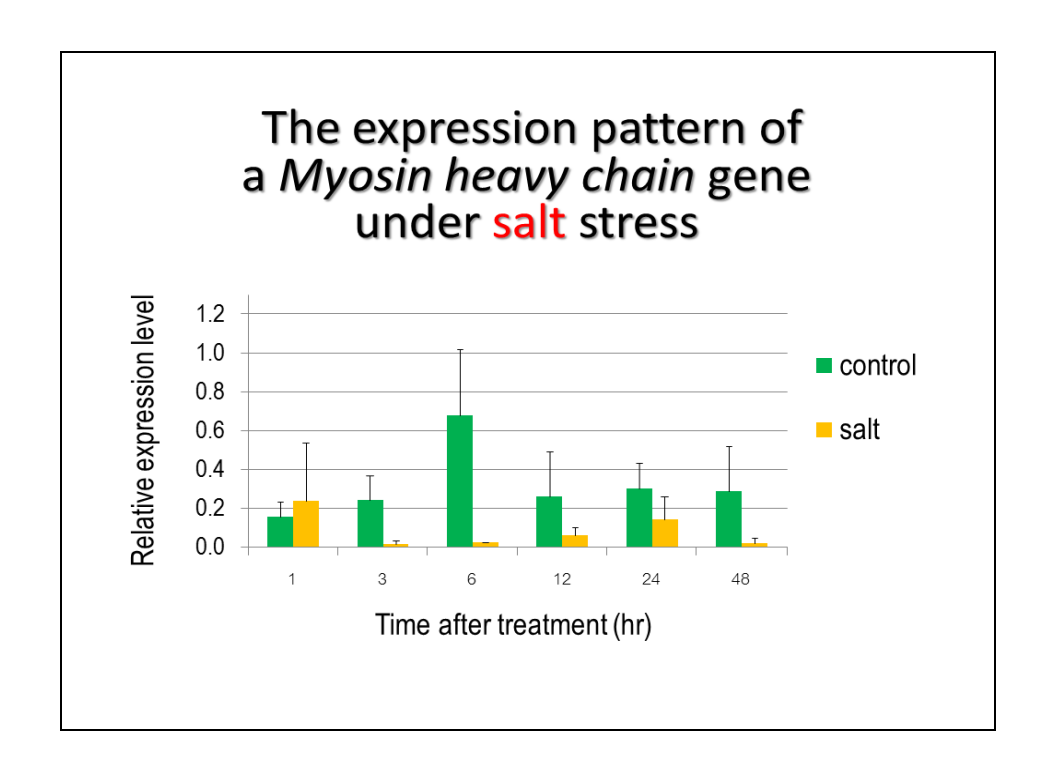


Figure 13 Interaction of OsMHCL protein with OsCaMs and OsCMLs examined by the yeast two-hybrid system. Yeast strain MaV203 co-transformed with the MHCL and CaM/CML constructs were grown at 30 $^{\circ}$ C for several days under selective (SC-LTH +100 mM 3AT containing either 50 mM CaCl₂ or 25 mM EGTA) condition. Serial dilutions of the transformed cells are shown by narrowing triangles.

5. Expression pattern of MHCL gene under salt and drought stress

The two-week-old 'KDML105' rice seedlings challenged by salt stress (150 mM NaCl) and drought stress (20% PEG6000) had survived for at least 48 hours within the experimental period. The expression level of *MHCL* gene compared to *EF1-alpha* as an internal control in leaf tissues after induction of salt stress was examined by real-time RT-PCR. The result showed that no significant change in the expression level of *MHCL* gene was detected under salt stress (Figure 14A). Under drought stress, significant difference in the expression level of *MHCL* gene was found at 6 hours after treatment, but at the other time points, no significant change in the expression level of *MHCL* gene was detected (Figure 14B).

A.



В.

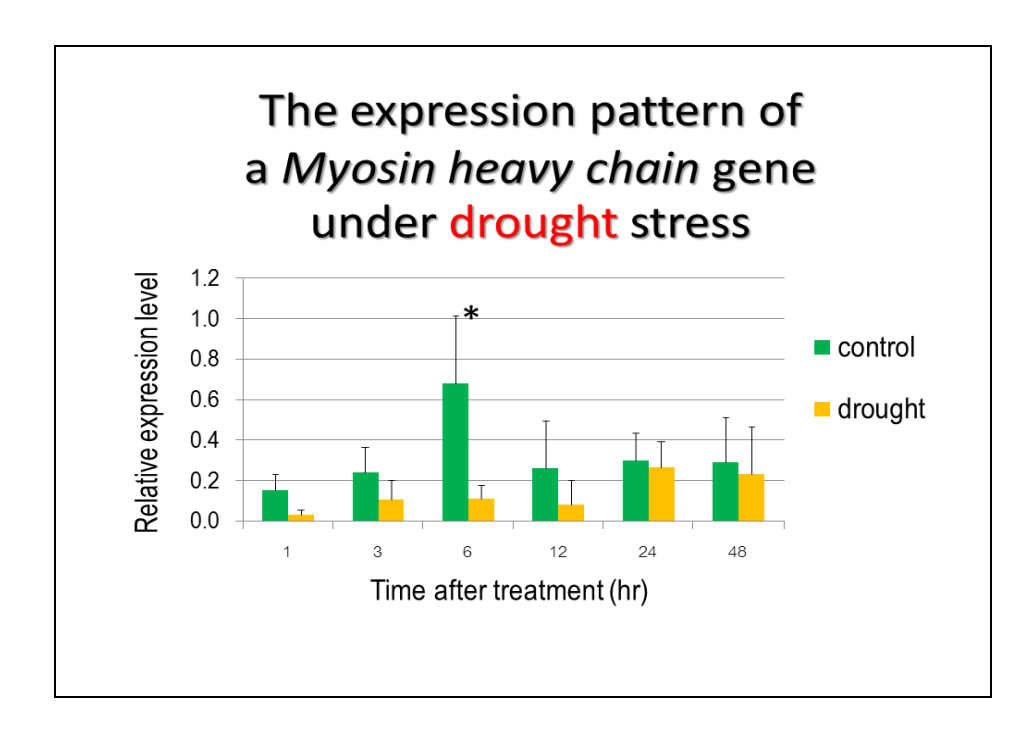


Figure 14 *MHCL* gene expression in the leaf of the 'KDML105' rice seedlings under salt stress (A), and drought stress (B) compared to those under normal conditions. Bar is the standard deviation (S.D.)

(* represent p<0.05).

6. Characterization of recombinant OsCML3 and its truncated form (OsCML3m)

The far-UV CD spectra of OsCML3 (Chinpongpanich et al, 2011) and OsCML3m in the presence of 1 mM CaCl₂ or 1 mM EGTA had two minima near 208 and 222 nm indicating that both proteins contain substantial α -helical secondary structure (Figure 15A-B). The molar ellipticity per residue for n amino acid residues ($[\theta]_n$) at 222 nm of rOsCML3m from the spectra in the presence of 1 mM CaCl₂ or 1 mM EGTA and their changes upon Ca²⁺ addition in comparison with that of rOsCML3 is summarized in Table 2, where Δ_{222} and % Δ_{222} are the absolute and percentage difference in $[\theta]_n$ at 222 nm between the presence and absence of Ca²⁺. Upon Ca²⁺ addition, an increase in $[\theta]_n$ at 222 nm was clearly observed for rOsCML3m with a 68.7 percent change while rOsCML3 showed a much smaller change in $[\theta]_n$ (10.5%). These results indicate that the helical content is highly increased in rOsCML3m protein upon Ca²⁺ binding.

In this study, ANS was used to measure the Ca²⁺-induced exposure of hydrophobic patches in the globular domains because its fluorescence spectrum is changed and can be monitored when it binds to the accessible hydrophobic surface of the proteins. The emission spectra of ANS when mixed with rOsCML3 or rOsCML3m in the presence of Ca²⁺ or EGTA are shown in Figure 15C-D. Table 2 summarizes the changes in ANS fluorescence in the presence of rOsCML3m upon Ca²⁺ addition in comparison with those of rOsCML3. When mixed with each protein in the presence of EGTA, ANS displayed a relatively weak fluorescence with a maximum wavelength near 520 nm, which is almost identical to that of ANS alone. In the presence of Ca²⁺, a significant blue shift (by 46 and 47 nm for rOsCML3 or rOsCML3m, respectively) in the maximum emission wavelength, was observed. Similar large increases in the fluorescence intensity of rOsCML3 (4.75-fold) and rOsCML3m (5.31-fold) were observed, suggesting that the 35-amino-acid CTE does not impede the exposure of its hydrophobic surface upon Ca²⁺ binding. However, in agreement with its smaller change in the increased helical content upon Ca²⁺ binding, exposure of the hydrophobic surface in rOsCML3.

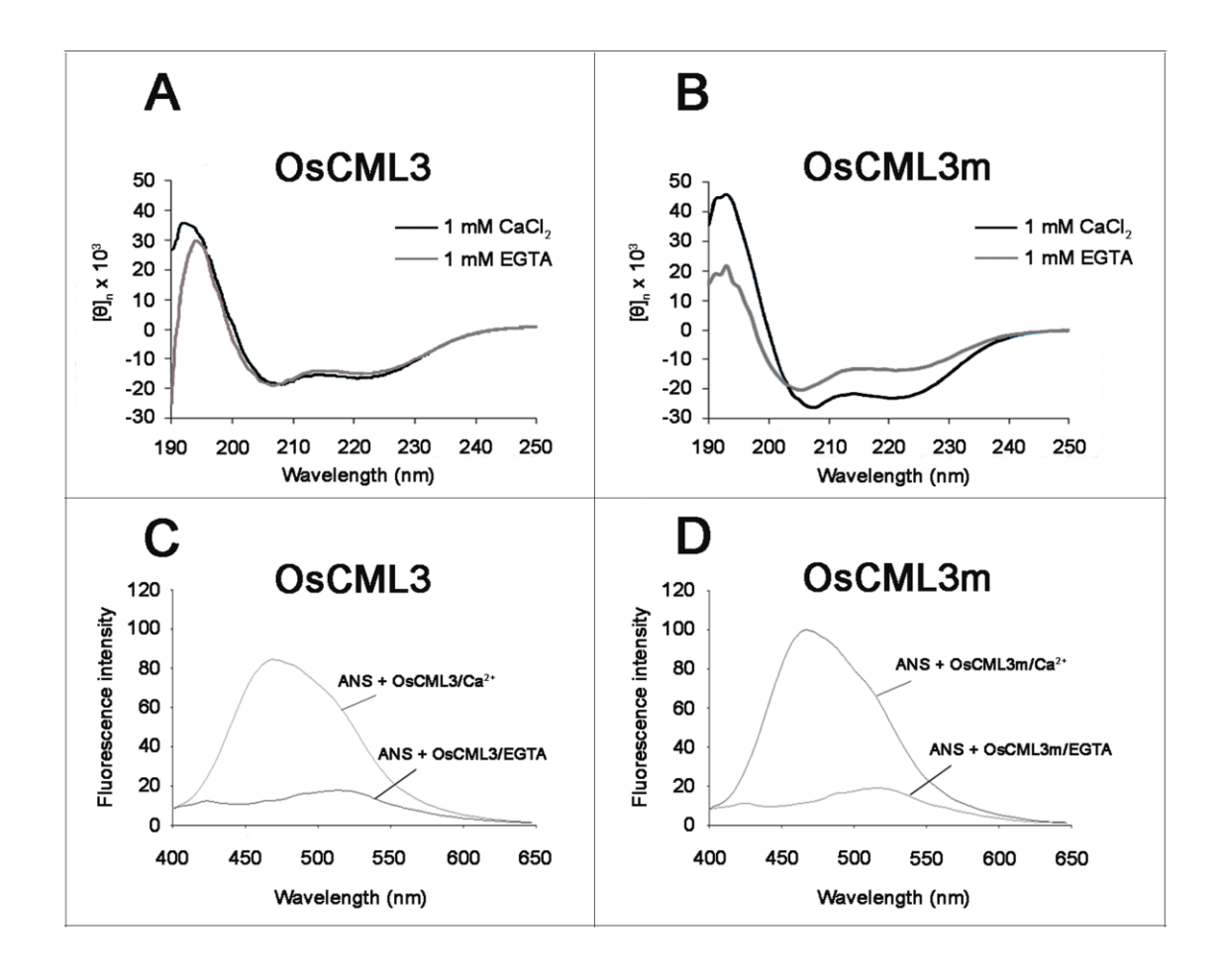


Figure 15 Ca²⁺-induced conformational changes of rOsCML3 and rOsCML3m. The far UV circular dischromism (CD) spectroscopy (A-B) and ANS fluorescence spectra (C-D) of rOsCML3m compared with those of rOsCML3 (published in Chiknpongpanich et al., 2011) were recorded in 1 mM Tris-HCl (pH 7.5) in the presence of 1 mM CaCl₂ or 1 mM EGTA. Spectra shown are representative of three independent experiments. In (A-B), $[\theta]_n$ is the molar ellipticity per residue for n amino acid residues.

7. OsCML3 localization

OsCML3 also has a potential prenylation site in the CTE domain, as described above, which may function in membrane association similar to OsCML1. To test whether the basic CTE domain containing the prenylation site imposed such a role on OsCML3, we determined the cellular localization of the CTE-truncated OsCML3m protein compared to the full-length protein (OsCML3). To examine the localization of OsCML3 and OsCML3m in planta, the pCAMBIA-GFP-OsCML3 and pCAMBIA-GFP-OsCML3m fusion constructs were individually introduced into Agrobacterium tumefaciens strain GV3101, and then into

tobacco leaf cells. The green fluorescence signal of GFP-CML3, which contained the CTE and putative prenylation site, was mostly observed in the plasma membrane of tobacco cells, while the GFP signal of GFP-CML3m (lacking the CTE and predicted prenylation site) was found in both the cytoplasm and the nucleus (Figure 16).

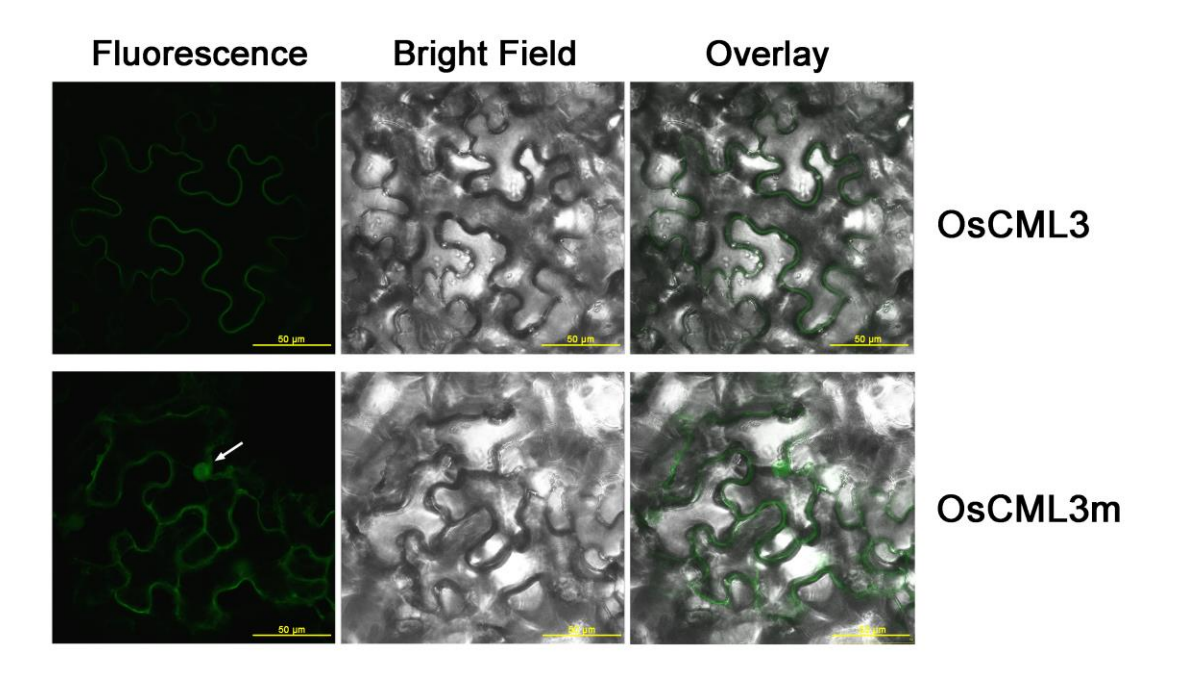


Figure 16 Subcellular localization of GFP-OsCML3 and GFP-OsCML3m in tobacco leaf cells. The green fluorescence, bright field and overlay images (60 x magnification) observed in tobacco leaf cells expressing the fusion proteins. Scale bar indicates 50 μ m. Images shown represent those seen from at least 100 such fields of view per sample and five independent samples. Nucleus was indicated with white arrow.

8. OsCML3 interaction with OsHMGB1, a novel target protein, in the nucleus

To identify target proteins of OsCML3, cDNA expression libraries were prepared from the leaf of *Oryza sativa* L. 'Khoa Dok Ma Li 105', and used for screening against rOsCML3m and rOsCML3 as described above. The results revealed that one of the ten putative novel OsCML3m-binding proteins was OsHMGB1. Note, however, that when the full-length rOsCML3 was used as the probe, only two target proteins were identified and these did not include OsHMGB1. Since chromosomal HMGB1 proteins are generally considered to be nuclear proteins (Grasser et al, 2007; Reeves, 2010). Although there is no experimental evidence on the subcellular localization of OsHMGB1, it was convincing from the theoretical predictions that the OsHMGB1 protein is localized in the nucleus.

The interaction between OsCML3 and its putative target, OsHMGB1 *in planta*, was evaluated using BiFC (Hu et al., 2002). The N-terminal fragment of yellow fluorescent protein (YFP) was fused with the N-terminal end of OsHMGB1 (YFP-HMGB1), while the C-terminal fragment of cyan fluorescent protein (CFP) was fused with the N-terminal end of OsCML3, OsCML3m or OsCML3s to yield CFP-CML3 or CFP-CML3m or CFP-CML3s, respectively. A green fluorescence signal was clearly observed in all combinations (OsHMGB1 with OsCML3, OsCML3m or OsCML3s) in the nucleus (Figure 17), confirming the interaction between OsCML3 and OsHMGB1 *in planta*. The interaction in the nucleus possibly occurred through the nuclear localization signal (NLS) of OsHMGB1. The N-terminal fragment of YFP or the C-terminal fragment of CFP, used as a negative control, yielded no fluorescent signal in leaf cells co-infiltrated with YFP and CFP-CML3, CFP-CML3m or CFP-CML3s, nor with YFP-HMGB1 and CFP.

9. OsCML3m inhibits OsHMGB1 binding to supercoiled DNA

The supercoiled DNA-binding property of rOsHMGB1 was examined by incubating supercoiled pUC19 plasmid (100 ng) with increasing concentrations of rOsHMGB1 (0-3 μM). That the pUC19 DNA interacted with rOsHMGB1 was shown by the resolved bands of lower electrophoretic mobility of the protein-DNA complex compared to that of the free DNA (Figure 18A). Examination of the effect of rOsCML3 or rOsCML3m upon the DNA-binding ability of rOsHMGB1 was evaluated by incubation of 1.0 µM of rOsHMGB1 and 100 ng of pUC19 at room temperature for 10 min and then adding increasing concentrations of rOsCML3 or rOsCML3m (0-2 μM). With increasing concentrations of rOsCML3, no effect on rOsHMGB1 binding to pUC19 was detected, as a similar rOsHMGB1 mobility shift as that without the addition of rOsCML3 was observed (Figure 18B). In contrast, the electrophoretic mobility of the rOsHMGB1-pUC19 complex increased in a dose-dependent manner in the presence of rOsCML3m from 0.1 µM (Figure 18C). Thus, only the CTE-truncated rOsCML3m affected the DNA-binding ability of rOsHMGB1. In addition, due to the high amino acid sequence identity shared with rOsCML3m, rOsCaM1 was tested under the same conditions to examine if rOsCaM1 could also interfere with the supercoiled DNA-binding ability of rOsHMGB1. However, like rOsCML3, rOsCaM1 had no effect on the rOsHMGB1 binding to supercoiled pUC19 (Figure 18D), indicating that the truncated (CTE-free) rOsCML3m specifically affected the supercoiled DNA-binding ability of rOsHMGB1. Without rOsHMGB1, rOsCML3, rOsCML3m and rOsCaM1 caused no mobility shift in the supercoiled pUC19 DNA (Figures 18E, 18F and 18G).

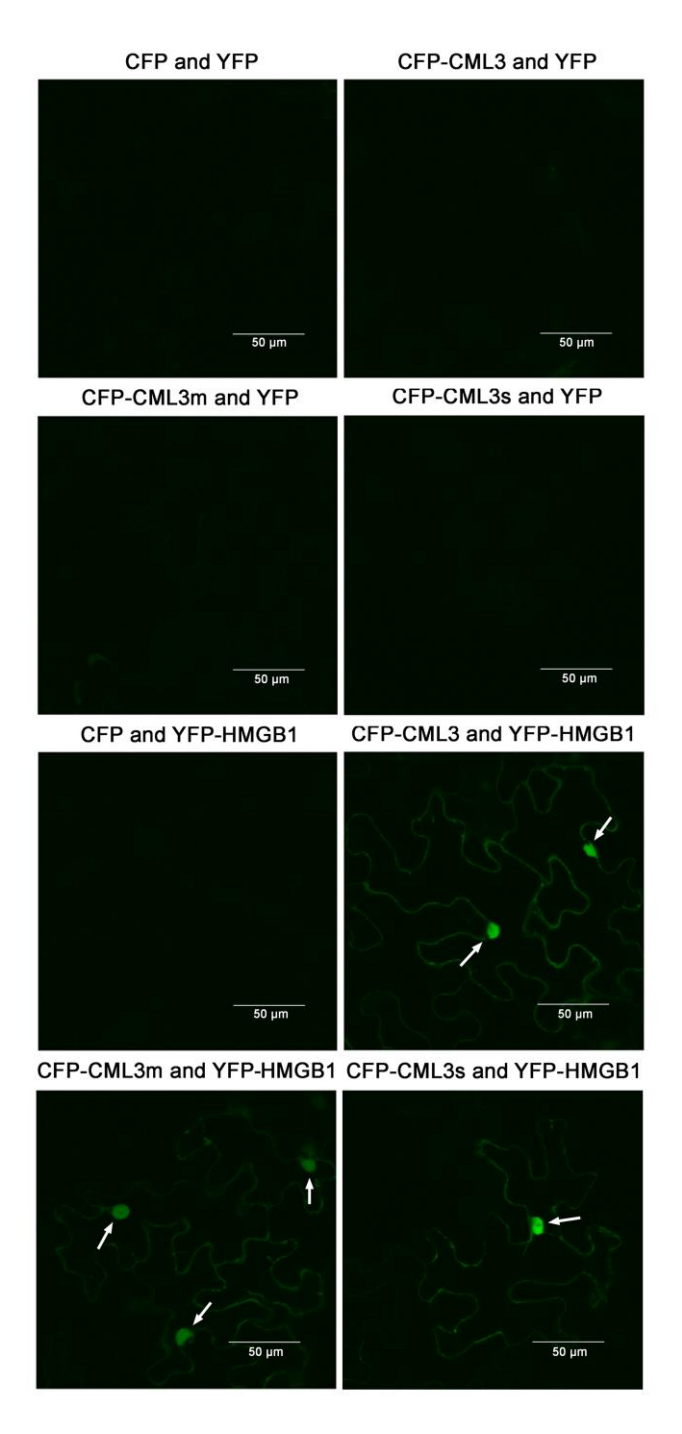


Figure 17 BiFC analysis of the OsHMGB1 interaction with OsCML3, OsCML3m and OsCML3s Fluorescent signals were observed in the nuclei of tobacco leaf cells. YFP and CFP represent the N-terminal fragment of yellow fluorescence protein and the C-terminal fragment of cyan fluorescence protein. As a control, Co-transformed constructs: of CFP and YFP, CFP-CML3 and YFP, CFP-CML3m and YFP, CFP-CML3s and YFP, and CFP and YFP-HMGB1were analyzed in parallel as the controls. Images shown represent those seen from at least 50 such fields of view per sample and five independent samples. Scale bars represent 50 μm. Nucleus was indicated with white arrow.

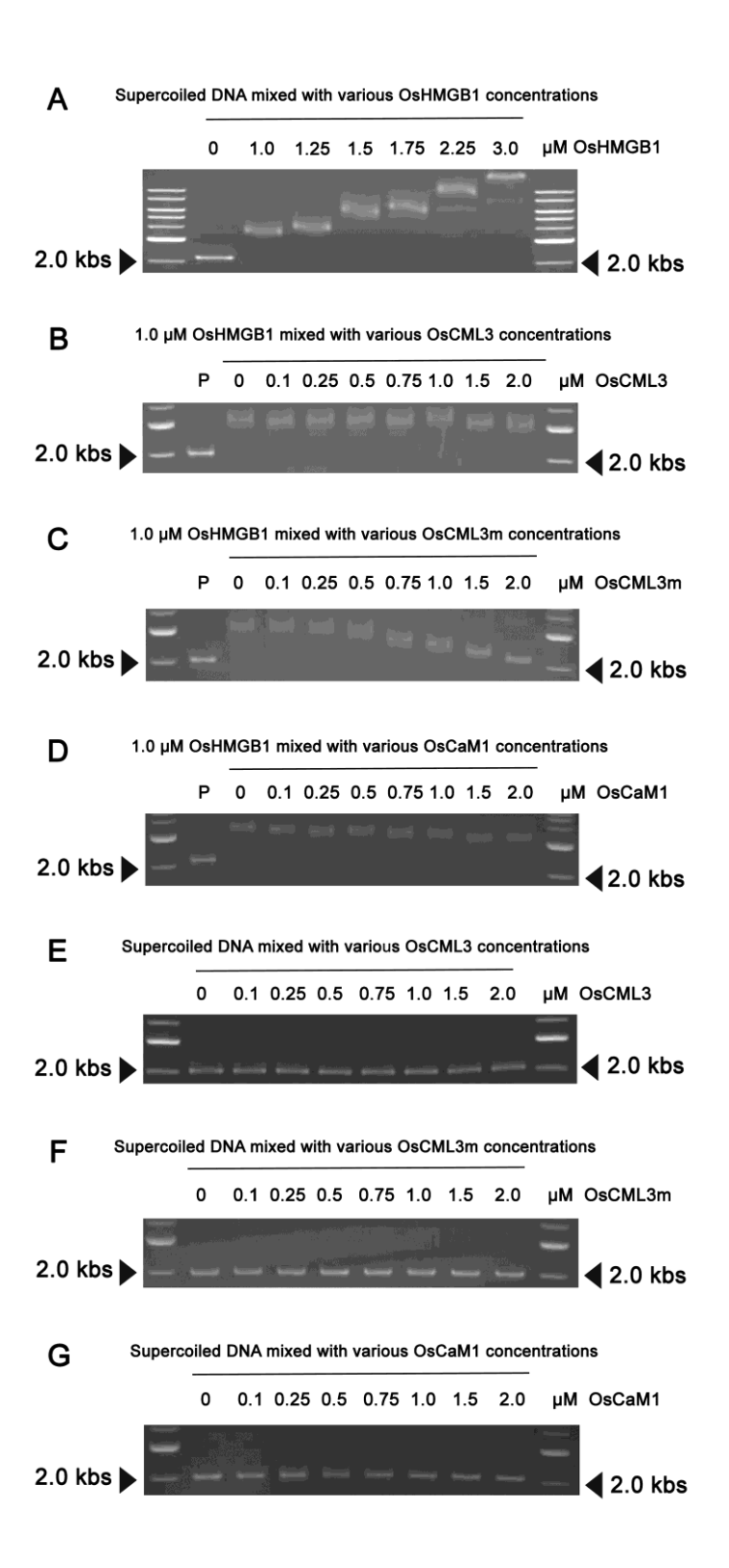


Figure 18 EMSA evaluation of the interaction of rOsHMGB1 with supercoiled pUC19 DNA (A) Various rOsHMGB1 concentrations (0–3.0 μ M) mixed with 100 ng supercoiled pUC19. (B–D) Mixtures of 1.0 μ M rOsHMGB1, supercoiled pUC19 (100 ng) and various rOsCML3, rOsCML3m or rOsCaM1concentrations (0–2.0 μ M). (E-G) Mixture of supercoiled pUC19 (100 ng) and various rOsCML3, rOsCML3m or rOsCaM1concentrations (0–2.0 μ M). Gels shown are representative of those seen from three independent repeats. Lane P represents pUC19 alone.

References

- Chinpongpanich A, Wutipraditkul N, Thairat S, Buaboocha T. Biophysical characterization of calmodulin and calmodulin-like proteins from rice, *Oryza sativa* L. *Acta Biochim Biophys Sin* 2011, 43: 867–876.
- Grasser KD, Launholt D, Grasser M. High mobility group proteins of the plant HMGB family: dynamic chromatin modulators. *Biochim Biophys Acta* 2007, 1769: 346-357.
- Hu CD, Chinenov Y, Kerppola TK. Visualization of interactions among bZIP and Rel family proteins in living cells using bimolecular fluorescence complementation. *Mol Cell* 2002, 9: 789-798.
- Langmead B, Trapnell C, Pop M, Salzberg SL. Ultrafast and memory-efficient alignment of short DNA sequences to the human genome. *Genome Biology* 2009, 10: R25.
- Mortazavi A, Williams BA, McCue K, Schaeffer L, Wold B. Mapping and quantifying mammalian transcriptomes by RNA-Seq. Nature Methods 2008, 5: 621-628.
- Ouyang S, Zhu W, Hamilton J, Lin H, Campbell M, Childs K, Thibaud-Nissen F, Malek RL, Lee Y, Zheng L, Orvis J, Haas B, Wortman J, Buell CR. The TIGR Rice Genome Annotation Resource: improvements and new features. *Nucleic Acids Res* 2007, 35: D883-D887.
- Qu B, Yin KQ, Liu SN, Yang Y, Gu T, Hui JMW, Zhang L, Miao J, Kondou Y, Matsui M, Gu HY, Qu LJ. A High-throughput screening system for *Arabidopsis* transcription factors and its application to Med25-dependent transcriptional regulation. *Mol Plant* 2011, 4: 546-555.
- Reeves R. Nuclear functions of the HMG proteins. Biochim Biophys Acta 2010, 1799: 3-14.
- Saeng-ngam S, Takpirom W, Buaboocha T, Chadchawan S. The role of the OsCam1-1 salt stress in ABA accumulation and salt tolerance in rice. *J Plant Biol* 2012, 55: 198-208.
- Thimm O, Bläsing O, Gibon Y, Nagel A, Meyer S, Krüger P, Selbig J, Müller LA, Rhee SY, Stitt M MAPMAN: a user-driven tool to display genomics data sets onto diagrams of metabolic pathways and other biological processes. *Plant J* 2004, 37:914-939.

Output ที่ได้จากโครงการวิจัย

1. ผลงานตีพิมพ์ในวารสารวิชาการนานาชาติ

Chinpongpanich A, Phean-o-pas S, ThongchuangM, Qu Li-Jia, Buaboocha T. C-Terminal Extension of Calmodulin-Like 3 Protein from *Oryza sativa* L.: Interaction with a High Mobility Group Target Protein. *Acta Bioch Bioph Sin* 2015, 47: 880-889

(Under preparation) Yuenyong W, ThongchuangM, Chinpongpanich A, Comai L, Chadchawan S, Buaboocha, T. Transcriptomics analysis of rice overexpressing the calcium sensor OsCaM1-1 revealed its effects on carbohydrate metabolism under salt stress.

2. การนำผลงานไปใช้ประโยชน์

โปรตีนคัลมอดุลินและโปรตีนคล้ายคัลมอดุลินเป็นกลุ่มโปรตีนรับสัญญาณแคลเซียมที่สำคัญและ มีหน้าที่ที่หลากหลายภายในเซลล์ยูคาริโอต โดยเฉพาะอย่างยิ่งในกลไกการตอบสนองต่อความเครียด จากสิ่งแวดล้อมของพืช ความรู้เกี่ยวกับการทำงานของโปรตีนกลุ่มนี้จากพืชยังมีน้อย ทั้งๆ ที่ในพืชที่มี การจำแนกหาโปรตีนกลุ่มนี้จากทั้งจีโนมแล้ว เช่น อะราบิดอปซิส ข้าว ซึ่งพบว่ามียีนจำนวนมากที่ สร้างโปรตีนคัลมอดุลินหรือโปรตีนสัญญาณแคลเซียมที่คล้ายคลึงกัน ดังนั้นการศึกษาการทำงานและ ความสำคัญในเชิงสรีรวิทยาของแต่ละยีนจึงมีความสำคัญที่จะช่วยให้เราเข้าใจกลไกในช่วงแรกของ การตอบสนองต่อสิ่งแวดล้อมของข้าวผ่านสัญญาณแคลเซียมที่อาศัยโปรตีนรับสัญญาณแคลเซียม เหล่านี้ เพื่อเป็นแนวทางในการใช้ประโยชน์จากยีนเหล่านี้ในการปรับปรุงพันธุ์ข้าวให้มีความสามารถ ในการต้านทานต่อความเครียดจากสิ่งแวดล้อมได้ต่อไป

3. การเชื่อมโยงกับต่างประเทศ

เกิดความร่วมมือทางการวิจัยกับนักวิจัยในต่างประเทศดังนี้

- 3.1 Professor Dr. Luca Comai, University of California, US
- 3.2 Professor Dr. Li-Jia Qu, Peking University, Beijing, China

ภาคผนวก



Acta Biochim Biophys Sin, 2015, 47(11), 880–889 doi: 10.1093/abbs/gmv097

Advance Access Publication Date: 29 September 2015

Original Article



Original Article

C-terminal extension of calmodulin-like 3 protein from *Oryza sativa* L.: interaction with a high mobility group target protein

Aumnart Chinpongpanich¹, Srivilai Phean-O-Pas¹, Mayura Thongchuang², Li-Jia Qu^{3,4}, and Teerapong Buaboocha^{1,*}

¹Department of Biochemistry, Faculty of Science, Chulalongkorn University, Bangkok 10330, Thailand, ²Division of Food Safety Management and Technology, Department of Science, Faculty of Science and Technology, Rajamangala University of Technology Krungthep, Bangkok 10120, Thailand, ³National Laboratory for Protein Engineering and Plant Genetic Engineering, College of Life Sciences, Peking University, Beijing 100871, China, and ⁴National Plant Gene Research Center (Beijing), Beijing 100101, China

*Correspondence address. Tel: +662-2185436; Fax: +662-2185418; E-mail: teerapong.b@chula.ac.th

Received 3 June 2015; Accepted 28 July 2015

Abstract

A large number of calmodulin-like (CML) proteins are present in plants, but there is little detailed information on the functions of these proteins in rice (Oryza sativa L.). Here, the CML3 protein from rice (OsCML3) and its truncated form lacking the C-terminal extension (OsCML3m) were found to exhibit a Ca²⁺-binding property and subsequent conformational change, but the ability to bind the CaM kinase II peptide was only observed for OsCML3m. Changes in their secondary structure upon Ca²⁺-binding measured by circular dichroism revealed that OsCML3m had a higher helical content than OsCML3. Moreover, OsCML3 was mainly localized in the plasma membrane, whereas OsCML3m was found in the nucleus. The rice high mobility group B1 (OsHMGB1) protein was identified as one of the putative OsCML3 target proteins. Bimolecular fluorescence complementation analysis revealed that OsHMGB1 bound OsCML3, OsCML3m or OsCML3s (cysteine to serine mutation at the prenylation site) in the nucleus presumably through the methionine and phenylalaninerich hydrophobic patches, confirming that OsHMGB1 is a target protein in planta. The effect of OsCML3 or OsCML3m on the DNA-binding ability of OsHMGB1 was measured using an electrophoretic mobility shift assay. OsCML3m decreased the level of OsHMGB1 binding to pUC19 doublestranded DNA whereas OsCML3 did not. Taken together, OsCML3 probably provides a mechanism for manipulating the DNA-binding ability of OsHMGB1 in the nucleus and its C-terminal extension provides an intracellular Ca²⁺ regulatory switch.

Key words: calcium, calmodulin (CaM), cell signaling, DNA-protein interaction, high mobility group

Introduction

Calcium signals play an important role in the response and adaptation to a variety of stimuli, including light, abiotic and biotic stresses, and hormones [1]. Changes of intracellular calcium levels are transduced through the stimulation of calcium ion (Ca²⁺) sensor proteins, one of which is the small multifunctional protein calmodulin (CaM) that

binds Ca^{2+} and alters the activity of a large number of target proteins in eukaryotes including plants. Structurally, CaM has two globular domains that are connected by a flexible α -helix, and each globular domain contains two Ca^{2+} -binding sites (EF-hands). Functionally, CaM regulates a variety of target proteins, including kinases, metabolic proteins, cytoskeletal proteins, ion channels and pumps, and transcription

factors [2]. Specific biological functions of plant CaMs are not well known [3], but plants possess a large family of unique CaM-like Ca²⁺-binding proteins (CMLs), most of which contain an EF-hand Ca²⁺-binding motif with no other identifiable functional domains. A large family of 50 CML genes in Arabidopsis (AtCML) [4] and 32 CML genes [5] in rice (OsCML) have been identified from their annotated genomes. Previously, AtCML24 (one of the first CMLs characterized) was shown to play a role in ion homeostasis, photoperiod-response, and abscisic acid-mediated inhibition of germination and seedling growth [6]. Moreover, AtCML43 and AtCML18 had been implicated in pathogen responses [7] and salinity tolerance [8], respectively. AtCML8 expression was shown to respond to salicylic acid or NaCl stress [9]. AtCML37, AtCML38, and AtCML39 play important roles as sensors in Ca²⁺-mediated developmental and stress response pathways [10]. These reports suggest that CMLs likely have diverse functions to interpret Ca2+ signals during development and stress responses.

In rice (Oryza sativa L.), 3 OsCaM and 32 OsCML proteins have been classified [5]. They are small proteins, consisting of 145-250 amino acid residues, and share an amino acid identity of 30.2-84.6% with OsCaM1. However, there is little information on the functional properties, subcellular localization, and transcriptional expression in different tissues and organelles, although OsCaM and OsCML genes showed differential expression patterns in different rice tissues or osmotic stresses [11]. OsCML31 (alias OsMSR2) was shown to confer enhanced tolerance to salt stress in transgenic Arabidopsis [12] and rice [13]. Interestingly, three OsCMLs contain a basic C-terminal extension (CTE) with a putative prenylation CAAX motif (C is cysteine, A is aliphatic, and X is a variety of amino acids) found as CVIL in OsCML1 and CTIL in OsCML2 and OsCML3. OsCML1 (alias OsCaM61) [14] was reported to be membrane-associated when it was prenylated and localized in the nucleus when it was unprenylated [15]. A similar protein, PhCaM53 previously found in petunia, also contained a basic CTE with a CAAX motif, and this was required for efficient prenylation in response to specific changes in carbon metabolism [16]. A similar subcellular localization of PhCaM53 in petunia was also reported to depend on its prenylation state.

As mentioned, there have been many CaM-binding proteins identified in plants [17], but no report of CML-binding proteins in rice is available. Here, the difference in biophysical characteristics and subcellular localization of OsCML3 and a truncated version of OsCML3 lacking the CTE (OsCML3m) were examined to investigate the effect of the CTE. To investigate the function of OsCML3, the rice high mobility group B1 (OsHMGB1), as one of the OsCML3-binding proteins, was identified and the interaction was verified using bimolecular fluorescence complementation (BiFC) assays. HMGB1 is a DNA-

binding protein that contains a non-specific sequence DNA-binding domain, which can bind to four-way junctions, cisplatin modified DNA and DNA minicircles [18]. HMGB1 functions as an architectural factor to facilitate the assembly of nucleoprotein complexes, and other DNA-dependent processes, which are involved in the regulation of transcription, recombination, and DNA repair [19,20–23]. Electrophoretic mobility shift assay (EMSA) was used to examine the DNA-binding ability of OsHMGB1 in the presence of OsCML3 or OsCML3m. A possible mechanism of the regulation of DNA-binding ability of OsHMGB1 via the action of OsCML3 was proposed.

Materials and Methods

Sequence retrieval and analysis

Nucleotide and amino acid sequences were obtained from the Gen-Bank database via the National Center for Biotechnology Information (http://www.ncbi.nlm.nih.gov/) [24], and the rice databases, including the MSU Rice Genome Annotation Project database [25] and the Rice Annotation Project Database [26]. Subcellular localization prediction was performed using the predicting plant protein subcellular location (Plant-PLoc) [27–30], Subnuclear Compartments Prediction System (Version 2.0) [31,32], and WoLF PSORT [33,34] programs.

Cloning, expression, and purification of recombinant OsCML3 and OsCML3m proteins

For OsCML3, the previously reported expression clone (OsCML3) [35] was used. The truncated clone of OsCML3 that lacked the sequence encoding the CTE, termed OsCML3m, was constructed by polymerase chain reaction (PCR) using the cDNA clone of the OsCML3 gene (AK111834) obtained from the DNA Bank of NIAS (Nagasaki Institute of Applied Science, Nagasaki, Japan) as the template and the OsCML3m primers (Table 1). PCR was performed using Phusion DNA polymerase (New England Biolabs, Ipswitch, USA) with thermal cycling for 30 cycles of 94°C for 5 min, 63°C for 1 min and 72°C for 1 min, and then a final 72°C for 10 min. The PCR product was cleaved and cloned into pET21a (Novagen, Darmstadt, Germany) using the selected restriction enzymes (NdeI and XhoI). The resulting selected clone was confirmed by DNA sequencing. Induction of recombinant protein production was performed in Escherichia coli BL21 (DE3) for 4 h by isopropyl β-D-thiogalactoside (IPTG) with a final concentration of 0.3 mM. The cells were then harvested, resuspended in 50 mM Tris-HCl buffer (pH 7.5) containing 0.5 mM dithiothreitol and 1 mM ethylenediaminetetraacetic acid (EDTA), sonicated and then centrifuged (27,000 g for 50 min at 4°C). Protein purification was performed using hydrophobic chromatography on

Table 1. Primers used for PCR in this study

| Gene name | Forward $(5' \rightarrow 3')$ | Reverse $(5' \rightarrow 3')$ | Used for |
|-----------|-------------------------------|-------------------------------|--------------------------|
| OsCML3m | CATATGGACCACCTGACAAA | ATCTCGAGTCATCGCTTTGCC | Protein expression |
| OsHMGB1 | CACCATGAAGGGGGCCAAATCC | TCACTCGTCATCGTCTTCATCC | BiFC assay |
| OsCML3 | CACCATGGACCACCTGACAAAGG | TCAGAGGATGGTACATGAGG | BiFC assay |
| OsCML3m | CACCATGGACCACCTGACAAAGG | TCACTTTGCCATCATGACCTTGAG | BiFC assay |
| OsCML3s | CACCATGGACCACCTGACAAAGG | TCAGAGGATGGTAGATGAGG | BiFC assay |
| OsHMGB1 | GGAATTCCATATGAAGGGGGCCAAATCC | CCGCTCGAGTCACTCGTCATCGTCTTC | EMSA |
| GFP | CCATGGTAGATCTGACTAGTAAAGG | GGTCACCAATCTCGAGGTGGTGGTGG | Subcellular localization |
| OsCML1 | CTCGAGGGTGGTGGCATGGCGG | GGTAACCTTACAGGATCACGCAC | Subcellular localization |
| OsCML1m | CTCGAGGGTGGTGGCATGGCGG | GGTTACCCTACTTGGCCATCATGC | Subcellular localization |
| OsCML3 | CTCGAGGGGGGGGGGAGGAATGGACC | GGTCACCTTTTTCAGAGGATGG | Subcellular localization |
| OsCML3m | CTCGAGGGGGGGGGGAGGAATGGACC | GGTTACCTTCACTTTGCCATCATGACC | Subcellular localization |

phenyl-Sepharose (Amersham, Little Chalfont, UK). Binding and washing were performed and proteins were eluted as previously reported [36]. The recombinant proteins were prepared as previously described [35]. All proteins samples were analyzed by 12% (w/v) SDS-polyacrylamide gel electrophoresis (PAGE) and then stained with Coomassie blue.

Electrophoretic shift analysis

To analyze the recombinant proteins by electrophoresis shift assay, a final concentration of 1 mM CaCl₂ or 3 mM ethyleneglycoltetraacetic acid (EGTA) was added to each protein solution (500 pmole), mixed and then resolved by SDS-PAGE with a 12.5% (w/v) acrylamide resolving gel. Proteins were then detected by Coomassie blue staining. To examine their peptide-binding ability, each protein (200 pmole) was mixed with the peptide derived from CaMKII (Sigma, St Louis, USA) at different molar equivalents and then analyzed as previously described [35].

Circular dichroism (CD) spectroscopy

CD spectroscopy was performed at 25°C in a J-715 Spectropolarimeter (Jasco, Easton, USA) with constant N_2 flushing. The farultraviolet (UV) CD spectrum was measured from 190 to 250 nm in 1 mM Tris–HCl (pH 7.5) and 1 mM KCl in the presence of 1 mM CaCl₂ or 1 mM EGTA. The final protein concentration was 10 μ M. All measurements were performed within 30 min after sample preparation, using a 1-mm-path-length quartz cell with a 1 s response time, 50 mdeg sensitivity, 50 nm/min scan speed, and a 2.0 nm spectral bandwidth. The average of three scans was taken. The secondary structure of the protein was estimated using K2D3 method (http://k2d3.ogic.ca//index.html) [37].

Fluorescence measurement

Measurement of the fluorescence emission spectra of 8-anilino-1-naphthalenesulphonate (ANS; Sigma) was performed on an LS55 Luminescence Spectrometer (PerkinElmer, Waltham, USA) at 25°C. Fluorescence emission spectra were monitored with an excitation wavelength light of 370 nm and emission spectra in the range 400–650 nm were scanned. All measurements were performed using $1\,\mu\text{M}$ of protein in 1 mM Tris–HCl (pH 7.5)/1 mM KCl with ANS at a final concentration of 100 μM in the presence of 1 mM CaCl₂ or 1 mM EGTA.

Screening of rice cDNA expression library

The ³⁵S-labeled purified rOsCML3 and rOsCML3m proteins were prepared as probes to screen a rice cDNA expression library. To construct the library, polyadenylated RNA was purified from the 'KDML105' rice total RNA using the GenElute mRNA Miniprep kit (Sigma) and then used as template for cDNA synthesis using the cDNA synthesis kit (Stratagene, La Jolla, USA). The Uni-ZAP XR Vector kit (Stratagene) was used to ligate the prepared rice cDNA to the lambda vector, resulting in the primary library. Primary, secondary, and tertiary screenings of the amplified library were performed. Single clones were excised and analyzed with the *Pst*I restriction enzyme. All unique pBluescript SK(+) plasmids obtained from the single-clone excision were sequenced. The obtained sequences were BLAST-searched against the Rice Genome Annotation Project and Rice Annotation Project databases to identify the cloned cDNA inserts.

Subcellular localization

To construct the pCAMBIA1302 containing either OsCML3 or OsCML3m fused with green fluorescent protein (GFP) at the N-terminal end, the coding region of OsCML3, OsCML3m, and GFP were amplified using the primers shown in Table 1. All PCR reactions were performed using Vent DNA polymerase (New England Biolabs) with 30 cycles of 94°C for 1 min, 59.3°C for 1 min and 72°C for 1 min and 30 s, and then followed by a final 72°C for 10 min. The resulting amplicons were cloned into the T&A cloning vector (RBC Bioscience Co., Taiwan, China) to give pTA-OsCML3, pTA-OsCML3m, and pTA-OsGFP, respectively. The gene fragments of OsCML3 and OsCML3m were individually inserted into pTA-OsGFP via the XhoI and BstEII sites at the 3' end of the GFP coding sequence, resulting in pTA-GFP-OsCML3 and pTA-GFP-OsCML3m, respectively. The fragments of GFP-OsCML3 and GFP-OsCML3m were sub-cloned into pCAMBIA1302 using NcoI and BstEII sites, resulting in pCAMBIA-GFP-OsCML3 and pCAMBIA-GFP-OsCML3m, respectively. The pCAMBIA1302 plasmids containing GFP-OsCML1 or GFP-OsCML1 m were also constructed and used for comparison. Each recombinant plasmid was introduced into Agrobacterium tumefaciens strain GV3101 by heat shock. The solution of Agrobacterium was then infiltrated into the leaf of tobacco plants and the plants were grown in the dark for 16 h followed by 48 h in the growth chamber. Confocal microscopy was performed with a Leica SPE microscope (Leica, Solms, Germany) using an excitation wavelength of 488 nm.

BiFC assay

The gene fragments of OsHMGB1 (AK062226), OsCML3, OsCML3m, and OsCML3s (serine-to-cysteine mutation at the prenylation site) were amplified by PCR using individual cDNA clones from the DNA Bank of NIAS (Nagasaki Institute of Applied Science) and the respective primer pairs (Table 1). All PCR reactions were performed using KOD DNA polymerase (Toyobo, Tokyo, Japan) with 35 cycles of 94°C for 1 min, 59°C for 45 s and 68°C for 1 min, and then followed by a final 68°C for 10 min. PCR products were ligated into the pENTR vector (Invitrogen, Carlsbad, USA) via a TOPO reaction, resulting in pENTR-HMGB1, pENTR-CML3, pENTR-CML3 m, and pENTR-CML3s, respectively. Then, the pcCFPxGW construct [38] was used to generate pCFP-CML3, pCFP-CML3 m, and pCFP-CML3s by LR Clonase™ II enzyme mix (LR recombination reactions) between pcCFPxGW and pENTR-CML3 or pENTR-CML3 m or pENTR-CML3s, respectively, and prepared as above. The pnYFPxGW construct [38] was also used to construct pYFP-HMGB1 by a similar reaction between pnYFPxGW and pENTR-HMGB1. Each pair of plasmids of pCFP-CML3 and pYFP-HMGB1, or pCFP-CML3 m and pYFP-HMGB1, or pCFP-CML3s and pYFP-HMGB1 was then co-transformed into Agrobacterium strain GV3101. The mixtures of the two Agrobacterium strains: GV3101 $(\mathrm{OD}_{600}$ = 0.5) and p19 $(\mathrm{OD}_{600}$ = 0.3) were co-infiltrated into the leaf of 6-week-old tobacco plants. The treated plants were grown in the dark for 16 h followed by 48 h in the growth chamber [38]. Confocal microscopy was performed with a Fluoview FV10i (Olympus, Tokyo, Japan) using an excitation wavelength of 488 nm.

Electrophoretic mobility shift assay (EMSA)

To generate the recombinant plasmid encoding HMGB1 fused with a His₆-Tag at the N-terminal end, PCR amplification by Phusion DNA polymerase (New England Biolabs) was performed using the cDNA clone for *OsHMGB1* as the template and the primer pair shown in **Table 1**. The PCR consisted of 30 cycles of 98°C for 7 s, 53°C for

20 s, and 72°C for 30 s, followed by a final 72°C for 10 min. The PCR product was cloned into pET28b. Protein production was performed in E. coli BL21 (DE3) for 4 h by IPTG with a final concentration of 0.4 mM. The cells were harvested and resuspended in binding buffer I [50 mM Tris-HCl buffer pH 7.5, 30 mM imidazole, 0.5 M NaCl, 0.5 mM dithiothreitol, 1 mM EDTA, and 1 x protease inhibitor mix (GE Healthcare, Waukesha, USA)]. Purification of rOsHMGB1 was performed by Ni-column chromatography (Amersham). The purified rOsHMGB1 (1.0 µM) was mixed in a final volume of 10 µl with 100 ng of pUC19 supercoiled DNA and various amounts (0-2.0 μM) of purified rOsCML3 or rOsCML3m (0-2.0 μM) in the presence of either 5 mM CaCl₂ or 2 mM EGTA in binding buffer [10 mM Tris-HCl pH 7.5, 50 mM NaCl, 1 mM DTT, 5% (v/v) glycerol, 0.05% (w/v) bromophenol blue, 0.05% (w/v) xylene cyanol] and then incubated at room temperature for 10 min. In addition, purified rOsCaM1, prepared previously [39], was incubated with rOsHMGB1 as above for direct comparison. The samples were analyzed by electrophoretic resolution in 1% (w/v) agarose-0.5 x Tris-borate-EDTA (TBE), and visualized under UV-light after ethidium bromide staining, as previously described [40].

Results

The 35-amino-acid CTE of OsCML3 interferes with its target protein binding

When the deduced amino acid sequences of *Oryza sativa* CaM-Like 3 (OsCML3) and its CTE-truncated form (OsCML3m) were compared by multiple sequence alignment with that of the rice CaM, OsCaM1, they were found to be highly similar (Fig. 1). All these proteins have four EF-hand domains and OsCML3 and OsCML3m shared 55.4 and 68.5% amino acid sequence identities with OsCaM1, respectively. In addition, OsCML3 contains a basic CTE domain with a putative prenylation CAAX (C is cysteine, A is aliphatic, and X is a variety of amino acids) motif (CTIL in OsCML3) [41].

To examine the role of the CTE, the rOsCML3m was produced and purified by Ca^{2+} -dependent hydrophobic chromatography using phenyl-Sepharose as shown in Fig. 2A. The apparent molecular weight (M_W) , derived from SDS-PAGE resolution, corresponded to the predicted M_W from the deduced amino acid sequence. One of the characteristics of a typical CaM is its ability to bind Ca^{2+} in the presence of SDS, which increases its electrophoretic mobility relative to that in the absence of Ca^{2+} . The rOsCML3m displayed this characteristic

mobility shift when incubated prior to electrophoresis with 1 mM Ca²⁺ compared with that with 3 mM EGTA (Fig. 2C). The degree of mobility shift of rOsCML3m appeared to be similar to that of the full-length OsCML3 as shown in Fig. 2B. When incubated with the CaM kinase II (CaMKII) peptide, a CaM-binding protein, rOsCML3m displayed a peptide–protein complex in the presence of Ca²⁺ (Fig. 2E), whereas rOsCML3 did not (Fig. 2D). In the absence of Ca²⁺, both proteins showed no binding ability to the peptide (data not shown). These results suggest that rOsCML3 has structural regions for binding the CaMKII peptide similar to those in CaM, but that the CTE domain appeared to obstruct this interaction.

The helical content upon Ca²⁺ binding of OsCML3 is affected by CTE

Far-UV CD spectrum was used to study whether secondary structure changes of OsCML3m occurred upon Ca2+ binding. Previously, major conformational changes, including an increase in α-helix upon Ca²⁺-binding, have been documented for CaM [42,43]. The far-UV CD spectra of OsCML3 (Fig. 3A) and OsCML3m (Fig. 3B) in the presence of 1 mM CaCl₂ or 1 mM EGTA had two minima near 208 and 222 nm indicating that both proteins contain substantial α-helical secondary structure. The molar ellipticity per residue for n amino acid residues ($[\theta]_n$) at 222 nm of rOsCML3m from the spectra in the presence of 1 mM CaCl2 or 1 mM EGTA with their calculated alpha helicity [37] and changes upon Ca2+ addition in comparison with that of rOsCML3 are summarized in Table 2, where Δ_{222} and % Δ_{222} are the absolute and percentage difference in $[\theta]_n$ at 222 nm between the presence and absence of Ca²⁺. Upon Ca²⁺ addition, an increase in $[\theta]_n$ at 222 nm was clearly observed for rOsCML3m with a 68.7% change while rOsCML3 showed a much smaller change in $[\theta]_n$ (10.5%). These results indicate that the helical content is highly increased in rOsCML3m protein upon Ca²⁺ binding.

In this study, ANS was used to measure the Ca²⁺-induced exposure of hydrophobic patches in the globular domains because its fluorescence spectrum is changed and can be monitored when it binds to the accessible hydrophobic surface of the proteins. The emission spectra of ANS when mixed with rOsCML3 [35] or rOsCML3m in the presence of Ca²⁺ or EGTA are shown in Fig. 3C,D, respectively. Table 3 summarizes the changes in ANS fluorescence in the presence of rOsCML3m upon Ca²⁺ addition in comparison with those of rOsCML3. When mixed with each protein in the presence of EGTA, ANS displayed a relatively weak fluorescence with a maximum

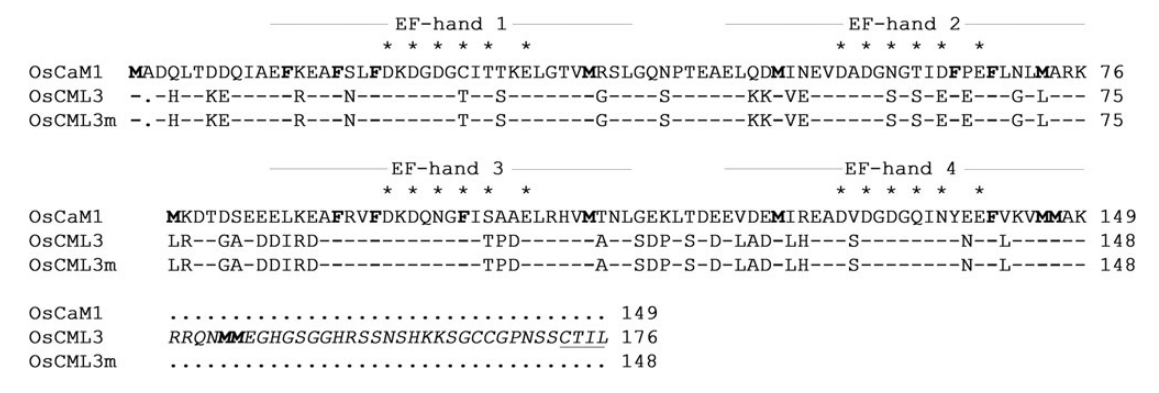


Figure 1. Comparison of the amino acid sequences of OsCML3 and OsCML3m with that of OsCaM1 by multiple sequence alignment The sequences are compared with OsCaM1 as a standard; identical residues are indicated by a dash (-), and a gap introduced for alignment purposes is indicated by a dot (.). Residues serving as Ca²⁺-binding ligands in the EF-hand motifs (EF-hand 1–4) are marked with an asterisk (*). Methionine (M) and Phenylanine (F) residues and the polybasic C-terminal extension (CTE) are shown in bold and italic, respectively. The CaaX box of OsCML3 for prenylation is underlined.

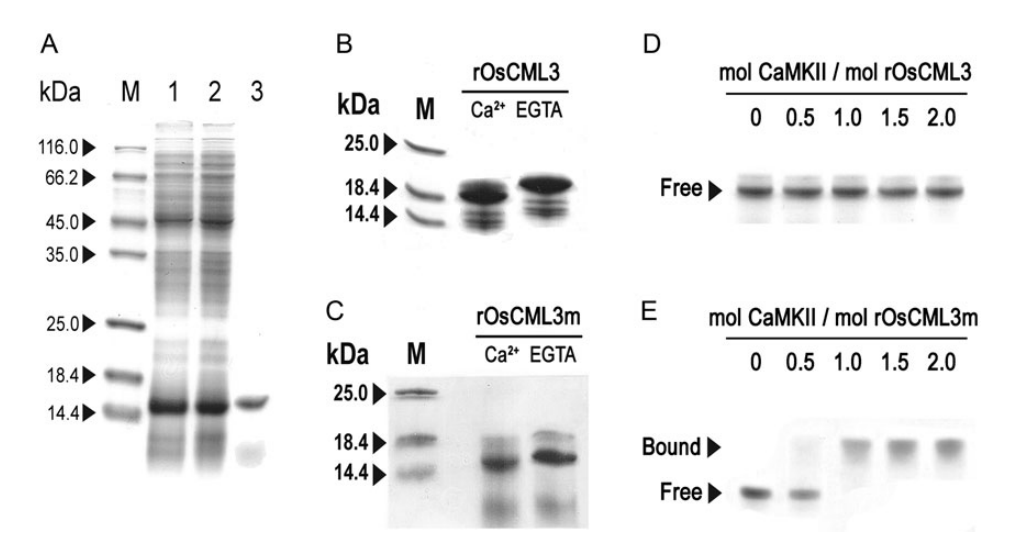


Figure 2. Analysis of the recombinant OsCML3m Representative protein patterns of *E. coli* BL21 (DE3) harboring pET21-OsCML3m detected by SDS-PAGE during recombinant protein purification by a phenyl-Sepharose column (A). Lane M, molecular mass standard proteins; lane 1, crude extract; lane 2, flow-through fraction; lane 3, eluted protein. Calcium-induced electrophoretic mobility shift analysis of rOsCML3 (B) and rOsCML3m (C). rOsCML3 and rOsCML3m proteins in the presence of 1 mM CaCl₂ (+Ca²⁺) or 3 mM EGTA (+EGTA) were subject to SDS-PAGE. Lane M, molecular mass standard proteins. Gel mobility shift analysis of rOsCML3 (D) and rOsCML3m (E) after incubation with increasing amounts of CaMKII peptide and in the presence of Ca²⁺ and then resolved by denaturing 4 M urea/SDS-PAGE. Gels shown are representative of three repeated experiments.

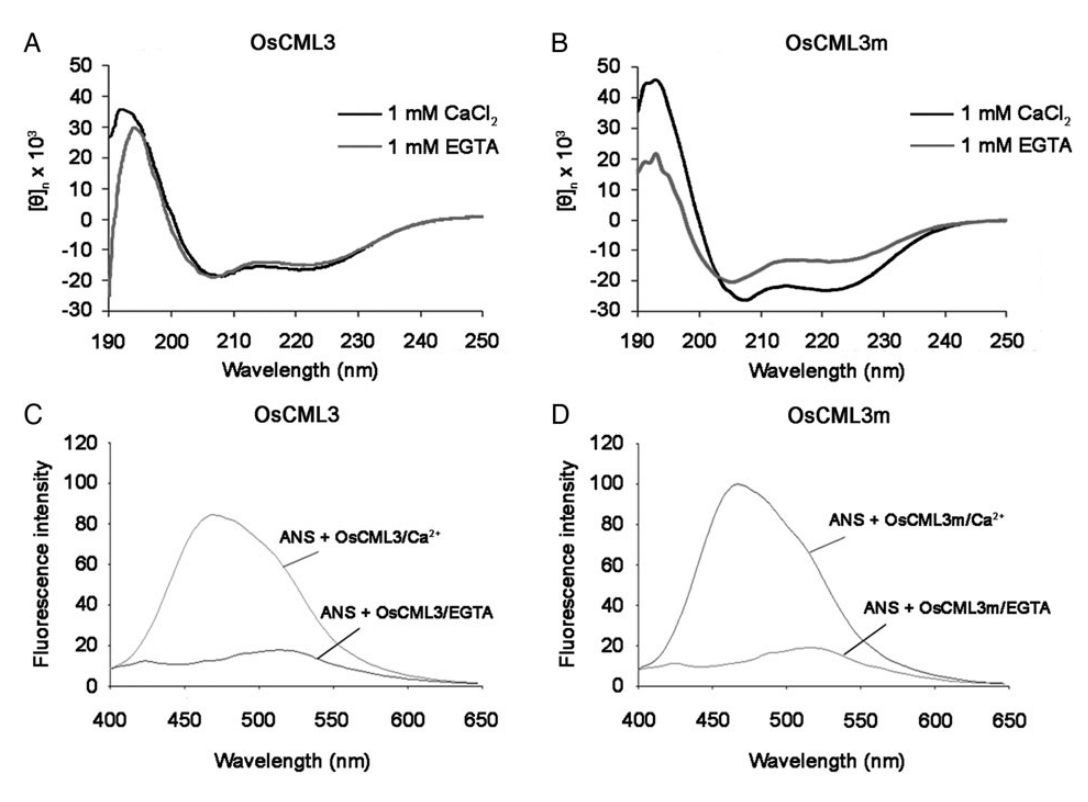


Figure 3. Ca^{2+} -induced conformational changes of rOsCML3 and rOsCML3m The far UV circular dischromism (CD) spectroscopy (A and B) and ANS fluorescence spectra (C and D) of rOsCML3m compared with those of rOsCML3 were recorded in 1 mM Tris–HCl (pH 7.5) in the presence of 1 mM CaCl₂ or 1 mM EGTA. Spectra shown are representative of three independent experiments. In (A and B), $[\theta]_n$ is the molar ellipticity per residue for n amino acid residues.

wavelength near 520 nm, which was almost identical to that of ANS alone. In the presence of Ca²⁺, a significant blue shift (46 and 47 nm for rOsCML3 or rOsCML3m, respectively) in the maximum emission wavelength was observed. Similar large increases in the fluorescence

intensity of rOsCML3 (4.75-fold) and rOsCML3m (5.31-fold) were observed, suggesting that the 35-amino-acid CTE does not impede the exposure of its hydrophobic surface upon Ca²⁺ binding. However, in agreement with its smaller change in the increased helical content

Table 2. Far-UV CD measurements of OsCML3 and OsCML3m

| Protein | $[\theta_n]_{222} \times 10^3 \ (deg.$ $cm^2/dmole.number$ of residues) ^a | | Δ_{222} | $\%\Delta_{222}$ | Alpha helicity (%) | |
|---------|--|---------------------|-------------------|-------------------|--------------------|-------|
| | +Ca ²⁺ | +EGTA | | | +Ca ²⁺ | +EGTA |
| OsCML3 | -16.31 ^b | -14.76 ^b | 1.55 ^b | 10.5 ^b | 49.08 | 36.35 |
| OsCML3m | -22.73 | -13.47 | 9.26 | 68.7 | 69.38 | 37.68 |

^aThe mean residue ellipticity at 222 nm.

Table 3. ANS fluorescence measurements of OsCML3 and OsCML3m

| Protein | Emission maximum (nm) | $\Delta \lambda_{\max}^a$ | I _{max} +Ca ²⁺ | +EGTA | I_{max} (+Ca ²⁺)/ I_{max} (+EGTA) ^b |
|---------|-----------------------------|---------------------------|---------------------------------------|--------------------|---|
| OsCML3 | 468° | 46° | 87.27 ^c | 18.37 ^c | 4.75° |
| OsCML3m | 467 | 47 | 101.37 | 19.09 | 5.31 |

 $^{^{}a}$ The difference in the maximum emission of ANS in the presence of Ca²⁺ and in the presence of EGTA.

upon Ca²⁺ binding, exposure of the hydrophobic surface in rOsCML3 occurred in such a way that it did not allow the protein to interact with the CaMKII peptide.

OsCML3 is localized to the plasma membrane via the CTE

OsCML1 (alias OsCaM61), the CML protein most similar to OsCML3 [14], was reported to be membrane-associated when prenylated and localized in the nucleus when unprenylated [15]. OsCML3 also has a potential prenylation site in the CTE domain, as described above, which may function in membrane association similar to OsCML1. To test whether the basic CTE domain containing the prenylation site played such a role in OsCML3, the cellular localization of the CTE-truncated OsCML3m protein compared with the full-length protein (OsCML3) was determined. By bioinformatics analysis using PlantLoc, WoLF PSORT, and Plant-mPLoc, OsCML3 and OsCML3m were predicted to localize in several compartments (data not shown), but the actual localization of OsCML3 and OsCML3m could not be concluded from these predictions. To examine the localization of OsCML3 and OsCML3m in planta, the pCAMBIA-GFP-OsCML3 and pCAMBIA-GFP-OsCML3m fusion constructs were individually introduced into A. tumefaciens strain GV3101, and then into tobacco leaf cells. The green fluorescence signal of GFP-CML3, which contained the CTE and putative prenylation site, was mostly observed in the plasma membrane of tobacco cells, while the GFP signal of GFP-CML3m (lacking the CTE and predicted prenylation site) was found in both the cytoplasm and the nucleus (Fig. 4).

OsCML3 interacts with OsHMGB1, a novel target for a Ca²⁺-binding protein, in the nucleus

To identify target proteins of OsCML3, cDNA expression libraries were prepared from the leaf of *Oryza sativa* L. 'Khoa Dok Ma Li 105', and used for screening against rOsCML3m and rOsCML3 as

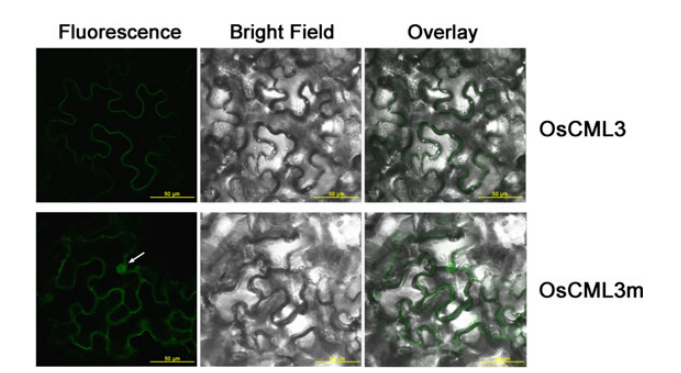


Figure 4. Subcellular localization of GFP-OsCML3 and GFP-OsCML3m in tobacco leaf cells
The green fluorescence, bright field, and overlay images ($60 \times \text{magnification}$) observed in tobacco leaf cells expressing the fusion proteins. Scale bar = $50 \, \mu \text{m}$. Images shown represent those seen from at least 100 such fields of view per sample and five independent samples. Nucleus was indicated with white arrow.

described above. The results revealed that one of the ten putative novel OsCML3m-binding proteins was OsHMGB1. However, when the full-length rOsCML3 was used as the probe, only two target proteins were identified and these did not include OsHMGB1. Since chromosomal HMGB1 proteins are generally considered to be nuclear proteins [44,45]. Although there is no experimental evidence on the subcellular localization of OsHMGB1, the theoretical predictions using three subcellular localization prediction programs similarly indicate that the OsHMGB1 protein is mainly localized in the nucleus.

The interaction between OsCML3 and its putative target, OsHMGB1 in planta, was evaluated using BiFC [46]. The N-terminal fragment of yellow fluorescent protein (YFP) was fused with the N-terminal end of OsHMGB1 (YFP-HMGB1), while the C-terminal fragment of cyan fluorescent protein (CFP) was fused with the N-terminal end of OsCML3, OsCML3m or OsCML3s to yield CFP-CML3 or CFP-CML3m or CFP-CML3s, respectively. A green fluorescence signal was clearly observed in all combinations (OsHMGB1 with OsCML3, OsCML3m or OsCML3s) in the nucleus (Fig. 5), confirming the interaction between OsCML3 and OsHMGB1 in planta. The interaction in the nucleus possibly occurred through the nuclear localization signal (NLS) of OsHMGB1. The N-terminal fragment of YFP or the C-terminal fragment of CFP, used as a negative control, yielded no fluorescent signal in leaf cells co-infiltrated with YFP and CFP-CML3, CFP-CML3m or CFP-CML3s, nor with YFP-HMGB1 and CFP.

OsCML3m but not OsCML3 inhibits OsHMGB1 binding to supercoiled DNA

The supercoiled DNA-binding property of rOsHMGB1 was examined by incubating supercoiled pUC19 plasmid (100 ng) with increasing concentrations of rOsHMGB1 (0–3 μM) in the presence of Ca $^{2+}$. The use of supercoiled DNA was to mimic the structure of DNA within the cells, which is packed and required for DNA/RNA synthesis. The pUC19 DNA interacted with rOsHMGB1 was shown by the resolved bands of lower electrophoretic mobility of the protein–DNA complex compared with that of the free DNA (Fig. 6A). The effect of rOsCML3 or rOsCML3m upon the DNA-binding ability of rOsHMGB1 was evaluated by incubation of 1.0 μM of rOsHMGB1 and 100 ng of pUC19 at room temperature for 10 min and then adding increasing concentrations of rOsCML3 or rOsCML3m (0–2 μM) in the presence of Ca $^{2+}$. With increasing concentrations of rOsCML3, no effect on

^bData obtained from Chinpongpanich et al. [35] for comparison.

^bThe ratio of the maximum fluorescence intensity of ANS in the presence of Ca²⁺ to that in the presence of EGTA.

^cData obtained from Chinpongpanich et al. [35] for comparison.

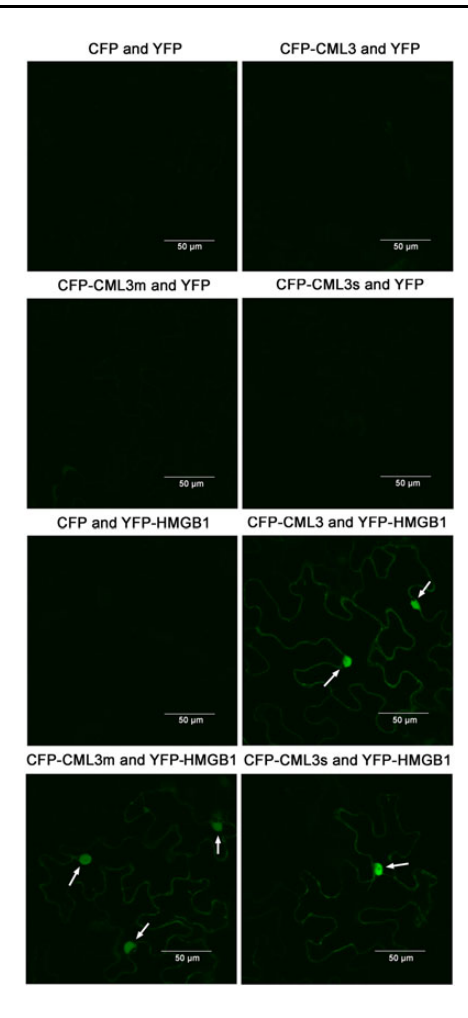


Figure 5. BiFC analysis of the OsHMGB1 interaction with OsCML3, OsCML3m, and OsCML3s. Fluorescent signals were observed in the nuclei of tobacco leaf cells co-infiltrated with a pair of *Agrobacterium* harboring YFP-HMGB1 and CFP-CML3, YFP-OsHMGB1 and CFP-CML3 m, or YFP-HMGB1 and CFP-CML3s. YFP represents the N-terminal fragment of yellow fluorescence protein (YFP) and CFP represents the C-terminal fragment of cyan fluorescence protein (CFP). Co-transformed constructs: CFP and YFP, CFP-CML3 and YFP, CFP-CML3 m and YFP, CFP-CML3s and YFP, and CFP and YFP-HMGB1 were analyzed in parallel as the controls. Images shown represent those seen form at least 50 such fields of view per sample and five independent samples. Scale bars represent 50 μm. Nucleus was indicated with white arrow.

rOsHMGB1 binding to pUC19 was detected, as a similar rOsHMGB1 mobility shift as that without the addition of rOsCML3 (Fig. 6B). In contrast, the electrophoretic mobility of the rOsHMGB1-pUC19 complex increased in a dose-dependent manner in the presence of rOsCML3m from 0.1 µM (Fig. 6C). Thus, only the CTE-truncated rOsCML3m affected the DNA-binding ability of rOsHMGB1. The inhibitory effect of the rOsCML3 was not observed in the absence of Ca²⁺ (data not shown). In addition, due to the high amino acid sequence identity shared with rOsCML3m, rOsCaM1 was tested under the same conditions to examine if rOsCaM1 could also interfere with the supercoiled DNA-binding ability of rOsHMGB1. However, like rOsCML3, rOsCaM1 had no effect on the rOsHMGB1 binding to supercoiled pUC19 (Fig. 6D), indicating that the truncated (CTEfree) rOsCML3m specifically affected the supercoiled DNA-binding ability of rOsHMGB1. Without rOsHMGB1, rOsCML3, rOsCML3m, and rOsCaM1 caused no mobility shift in the supercoiled pUC19 DNA (Fig. 6E-G).

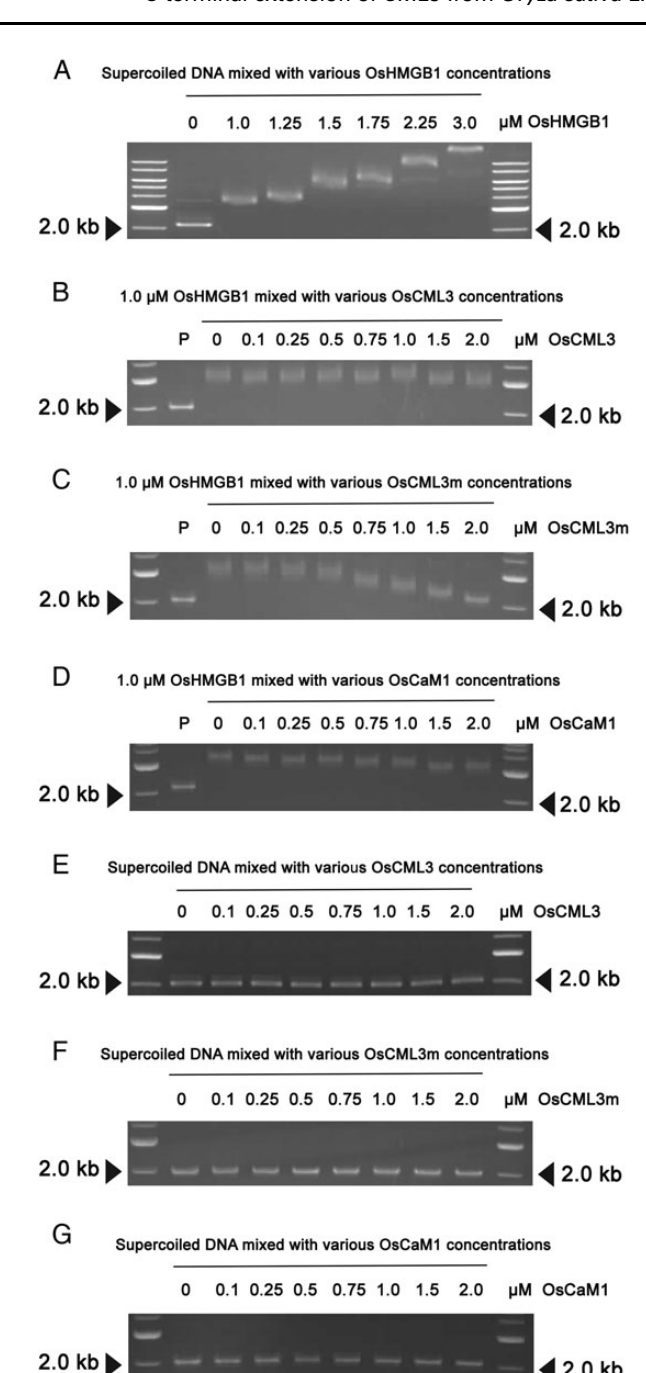


Figure 6. Electrophoretic mobility shift assay of the interaction of rOsHMGB1 with supercoiled pUC19 DNA (A) Various rOsHMGB1 concentrations (0–3.0 μ M) mixed with 100 ng supercoiled pUC19. (B–D) Mixtures of 1.0 μ M rOsHMGB1, supercoiled pUC19 (100 ng) and various rOsCML3, rOsCML3m, or rOsCaM1concentrations (0–2.0 μ M). (E–G) Mixture of supercoiled pUC19 (100 ng) and various rOsCML3, rOsCML3m, or rOsCaM1 concentrations (0–2.0 μ M). Gels shown are representative of those seen from three independent repeats. Lane P represents pUC19 alone.

Discussion

The use of Ca²⁺-dependent phenyl-Sepharose hydrophobic chromatography to successfully purify rOsCML3 [35] and rOsCML3m was based upon the presence of several methionines and other hydrophobic amino acids, which constitute the hydrophobic patches that are exposed in the Ca²⁺-bound form. Both OsCML3 and OsCML3m

exhibited the characteristic electrophoretic gel mobility shift and similar changes in the ANS fluorescence spectra in the presence of Ca²⁺. These results suggest that the polybasic CTE had no apparent effect on the ability of OsCML3 to bind Ca²⁺ and to expose the hydrophobic regions.

Examination of the OsCML3 CD spectra showed a relatively small change in the $[\theta]_n$ at 208 and 222 nm upon Ca²⁺ binding, similar to that previously observed with OsCML1 [35]. In contrast, OsCML3m displayed a significant change, indicating a large increase in the helical content of OsCML3m upon Ca²⁺ binding. Within the CTE, the apo form of OsCML1 (alias OsCaM61) was previously reported to have an extended final helix compared with the holo form, but the Ca²⁺-bound form seemed to have a much shorter final helix that became flexible in the Ca²⁺-saturated protein [47]. OsCML3 was predicted to have an extended final helix as well (data not shown), but it was shorter than that of OsCML1 suggesting that, if both proteins behave similarly upon Ca²⁺ binding, the increased helical content of OsCML3 likely comes from other parts of the protein. Supported from previous reports, the increased helical content may be resulted from the central α-helix becoming more structured upon Ca²⁺ binding [48], which may be inhibited by the presence of the CTE, thus the smaller change observed in the $[\theta]_n$ from full-length OsCML3. These results suggest that the CTE of OsCML3 has regulatory effects on Ca2+-induced conformational changes, and in turn upon the specific binding of OsCML3 to its targets, in which the hydrophobic patches and the helices surrounding the Ca²⁺-binding loops are very important [49–51].

Interestingly, OsCML3m interacted with the CaM-binding peptide derived from CaMKII while the full-length OsCML3 did not. Thus, the CaM-like region of OsCML3 could interact with the CaM-KII peptide upon a Ca²⁺-induced conformational change similar to typical CaMs, but the CTE appeared to obstruct this interaction suggesting that the CTE interacts with the rest of the protein. A previous nuclear magnetic resonance study indicated that the CTE of OsCML1 indeed interacted with the rest of the protein, leading to a decreased flexibility of this region [47]. The truncated OsCML1 without its CTE was shown to possess a higher ability to activate MLCK and CaMKII compared with that of the full-length OsCML1, supporting the inhibitory effect of the CTE [15].

For other target proteins, the CTE of OsCML1 has been reported to decrease the activation of phosphodiesterase [2]. In contrast, OsCML1 was reported to activate the CaM-binding protein kinases (OsCBKs) in a Ca²⁺-dependent manner, while the CTE domain was not required for this effect [52]. These results suggest a differential activity of the CTE domain upon the binding ability of these CML proteins to different target proteins. Nonetheless, the CTE likely plays regulatory roles in the Ca²⁺-modulated activity of these CML proteins. For OsCML3, to overcome the interfering effect of its CTE *in vivo*, we hypothesized that other proteins or mechanisms may be involved in the target binding of OsCML3, or that there are post-translation modifications of either OsCML3 or its target protein or both proteins to facilitate their interaction.

OsHMGB1 was found to be one of the putative targets of OsCML3m by screening a cDNA expression library with OsCML3m as the probe. Screening with the full-length OsCML3 identified only a few targets and not OsHMGB1, which conforms to the notion that the CTE interferes with target binding of OsCML3. The BiFC assay showed that OsHMGB1–OsCML3, OsHMGB1–OsCML3m, and OsHMGB1–OsCML3s interactions all occurred in the nucleus. The NLS of OsHMGB1 likely facilitated the movement of these protein complexes to the nucleus. Possibly, either unknown proteins or mechanisms are involved in exposing specific regions of OsCML3 for

binding to OsHMGB1, or that post-translational modification of OsHMGB1 or OsCML3 facilitates the interaction. The latter scenario has been observed from the phosphorylation of maize HMGB1 by protein kinase CK2 that abolishes its interaction with transcription factor Dof2 and the stimulation of Dof2 DNA binding [53] or the methylation and phosphorylation of CaM, which affect its activity for binding to target proteins [54–56].

In general, HMGB proteins are known to play a role in the regulation of transcription and other DNA-dependent processes [19,21,45], and OsHMGB was observed to accumulate in cold-treated rice seedlings [57] while over-expression of AtHMGB2 reduced seed germination under dehydration conditions in Arabidopsis [58]. These results indicated that HMGB proteins likely play a role in the responses to various stresses, possibly through DNA-binding dependent processes. Here, the examination of the effect of OsCML3 or OsCML3m on the binding of OsHMGB1 to supercoiled DNA revealed that OsCML3m decreased the binding of OsHMGB1 and supercoiled pUC19 DNA in the presence of Ca²⁺, while OsCML3 did not. These findings indicated that in vitro the CTE of OsCML3 inhibits its binding ability to OsHMGB1. Since the interaction between OsCML3 and OsHMGB1 was observed in the nucleus, we speculate that, probably with the help of other proteins or unknown mechanisms, the inhibitory effect of the CTE is released leading to the interaction of OsCML3 with OsHMGB1 and the transport of the complex into the nucleus, where OsCML3 might function to regulate the DNA binding of OsHMGB1 in the nucleus and subsequently affect transcription and other DNA-dependent processes [19,21,45].

Overall, OsCML3 and OsCML3m both possessed Ca2+-binding ability, but exhibited differences in their changes in the CD-spectra upon Ca²⁺ binding, where OsCML3m showed a larger increase in the helical content. It is suggested that the CTE affects the Ca² +-induced conformational change of OsCML3. Exposure of the hydrophobic patches was observed for both OsCML3 and OsCML3m; however, the CTE of OsCML3 appeared to influence the Ca2+-induced conformational change in such a way that OsCML3 cannot interact with OsHMGB1 (identified here as a novel target for Ca2+ sensor proteins). In planta, OsHMGB1 interacted with OsCML3m as well as with full-length OsCML3 in the nucleus, suggesting a mechanism for releasing the inhibitory effect of the CTE exists in the cytosol. OsCML3 is then likely brought into the nucleus through the NLS of OsHMGB1. Moreover, the supercoiled DNA-binding ability of OsHMGB1 was interfered by the presence of OsCML3m in the presence of Ca²⁺. Taken together, OsCML3 may provide a mechanism for manipulating the DNA-binding ability of OsHMGB1 in the nucleus with the CTE providing an intracellular Ca²⁺ regulatory switch.

Acknowledgements

We would like to thank Assistant Professor Dr Kuakarun Krusong, Department of Biochemistry, Faculty of Science, Chulalongkorn University for advice and Dr Robert Bucher, PCU, Faculty of Science, Chulalongkorn University, for useful comments, and English proofreading and editing.

Funding

This work was supported by Thailand Research Fund (No. BRG5680019) to T.B. A.C. was supported by the Royal Golden Jubilee Ph.D. program-RGJ (No. 4.C.CU/53.G.1/P.XX) from the

Thailand Research Fund and Chulalongkorn University Centenary Academic Development Project. Additional support was provided for the research group 'Special Task Force for Activating Research (STAR): Biochemical and Molecular Mechanisms of Rice in Changing Environments' (No. GSTAR 57-005-23-002) by the Ratchadaphisek-sompot Endowment Fund, Chulalongkorn University and Thailand Research Fund (No. IRG5780008) (to T.B.).

References

- 1. Yang T, Poovaiah BW. Calcium/calmodulin-mediated signal network in plants. *Trends Plant Sci* 2003, 8: 505–512.
- Bouche N, Yellin A, Snedden WA, Fromm H. Plant-specific calmodulinbinding proteins. Annu Rev Plant Biol 2005, 56: 435–466.
- Yoo JH, Park CY, Kim JC, Heo WD, Cheong MS, Park HC, Kim MC, et al. Direct interaction of a divergent CaM isoform and the transcription factor, MYB2, enhances salt tolerance in Arabidopsis. J Biol Chem 2005, 280: 3697–3706.
- McCormack E, Braam J. Calmodulins and related potential calcium sensors of Arabidopsis. New Phytol 2003, 159: 585–598.
- Boonburapong B, Buaboocha T. Genome-wide identification and analyses of the rice calmodulin and related potential calcium sensor proteins. BMC Plant Biol 2007, 7: 4.
- Delk NA, Johnson KA, Chowdhury NI, Braam J. CML24, regulated in expression by diverse stimuli, encodes a potential Ca²⁺ sensor that functions in responses to abscisic acid, daylength, and ion stress. *Plant Physiol* 2005, 139: 240–253.
- Chiasson D, Ekengren SK, Martin GB, Dobney SL, Snedden WA. Calmodulin-like proteins from *Arabidopsis* and tomato are involved in host defense against *Pseudomonas syringae* pv. *Plant Mol Biol* 2005, 58: 887–897.
- Yamaguchi T, Aharon GS, Sottosanto JB, Blumwald E. Vacuolar Na⁺/H⁺ antiporter cation selectivity is regulated by calmodulin from within the vacuole in a Ca²⁺- and pH-dependent manner. *Proc Natl Acad Sci USA* 2005, 102: 16107–16112.
- Park HC, Park CY, Koo SC, Cheong MS, Kim KE, Kim MC, Lim CO, et al. AtCML8, a calmodulin-like protein, differentially activating CaMdependent enzymes in Arabidopsis thaliana. Plant Cell Rep 2010, 29: 1297–1304.
- Vanderbeld B, Snedden WA. Developmental and stimulus-induced expression patterns of *Arabidopsis* calmodulin-like genes CML37, CML38 and CML39. Plant Mol Biol 2007, 64: 683–697.
- Chinpongpanich A, Limruengroj K, Phean-o-pas S, Limpaseni T, Buaboocha T. Expression analysis of calmodulin and calmodulin-like genes from rice, Oryza sativa L. BMC Res Notes 2012, 5: 625.
- Xu GY, Rocha PS, Wang ML, Xu ML, Cui YC, Li LY, Zhu YX, et al. A novel rice calmodulin-like gene, OsMSR2, enhances drought and salt tolerance and increases ABA sensitivity in Arabidopsis. Planta 2011, 234: 47–59.
- Xu GY, Cui YC, Li MJ, Wang ML, Yu Y, Zhang B, Huang LF, et al. OsMSR2, a novel rice calmodulin-like gene, confers enhanced salt tolerance in rice (Oryza sativa L.). Aust J Crop Sci 2013, 7: 368–373.
- Xiao C, Xin H, Dong A, Sun C, Cao K. A novel calmodulin-like protein gene in rice which has an unusual prolonged C-terminal sequence carrying a putative prenylation site. DNA Res 1999, 6: 179–181.
- Dong A, Xin H, Yu Y, Sun C, Cao K, Shen WH. The subcellular localization of an unusual rice calmodulin isoform, OsCaM61, depends on its prenylation status. *Plant Mol Biol* 2002, 48: 203–210.
- Rodríguez-Concepción M, Yalovsky S, Zik M, Fromm H, Gruissem W. The prenylation status of a novel plant calmodulin directs plasma membrane or nuclear localization of the protein. EMBO J 1999, 18: 1996–2007.
- Snedden WA, Fromm H. Calmodulin, calmodulin-related proteins and plant responses to the environment. *Trends Plant Sci* 1998, 3: 299–304.
- Wu Q, Zhang W, Pwee KH, Kumar PP. Cloning and characterization of rice HMGB1 gene. Gene 2003, 312: 103–109.
- Agresti A, Bianchi ME. HMGB proteins and gene expression. Curr Opin Genet Dev 2003, 13: 170–178.

- Bustin M. Regulation of DNA-dependent activities by the functional motifs
 of the high-mobility-group chromosomal proteins. Mol Cell Biol 1999, 19:
 5237–5246.
- Bustin M, Reeves R. High-mobility-group chromosomal proteins: architectural components that facilitate chromatin function. *Prog Nucleic Acid Res Mol Biol* 1996, 54: 35–100.
- Grasser KD. Chromatin-associated HMGA and HMGB proteins: versatile co-regulators of DNA-dependent processes. *Plant Mol Biol* 2003, 53: 281–295.
- Thomas JO, Travers AA. HMG1 and 2, and related "architectural" DNAbinding proteins. Trends Biochem Sci 2001, 26: 167–174.
- Benson DA, Cavanaugh M, Clark K, Karsch-Mizrachi I, Lipman DJ,
 Ostell J, Sayers EW. GenBank. Nucleic Acids Res 2013, 41: D36–D42.
- Ouyang S, Zhu W, Hamilton J, Lin H, Campbell M, Childs K, Thibaud-Nissen F, et al. The TIGR rice genome annotation resource: improvements and new features. Nucleic Acids Res 2007, 35: D883–D887.
- Tanaka T, Antonio BA, Kikuchi S, Matsumoto T, Nagamura Y, Numa H, Sakai H. The rice annotation project database (RAP-DB) update. *Nucleic Acids Res* 2008, 36: D1028–D1033.
- Chou KC. Using amphiphilic pseudo amino acid composition to predict enzyme subfamily classes. *Bioinformatics* 2005, 21: 10–19.
- Chou KC, Shen HB. Large-scale plant protein subcellular location prediction. J Cell Biochem 2007, 100: 665–678.
- Chou KC, Shen HB. Cell-PLoc: a package of web-servers for predicting subcellular localization of proteins in various organisms. *Nat Protoc* 2008. 3: 153–162.
- Shen HB, Chou KC. Ensemble classifier for protein folding pattern recognition. Bioinformatics 2006, 22: 1717–1722.
- Lei Z, Dai Y. An SVM-based system for predicting protein subnuclear localizations. BMC Bioinformatics 2005, 6: 291.
- 32. Lei Z, Dai Y. Assessing protein similarity with Gene Ontology and its use in subnuclear localization prediction. *BMC Bioinformatics* 2006, 7: 491.
- Horton P, Park KJ, Obayashi T, Nakai K. Protein subcellular localization prediction with WoLF PSORT. Proceedings of the 4th Annual Asia Pacific Bioinformatics Conference APBC06, Taipei, China, 2006, pp 39–48.
- Horton P, Park KJ, Obayashi T, Fujita N, Harada H, Adams-Collier CJ, Nakai K. WoLF PSORT: protein localization predictor. *Nucleic Acids Res* 2007, 35: W585–W587.
- Chinpongpanich A, Wutipraditkul N, Thairat S, Buaboocha T. Biophysical characterization of calmodulin and calmodulin-like proteins from rice, Oryza sativa L. Acta Biochim Biophys Sin 2011, 43: 867–876.
- Liao B, Zielinski RE. Production of recombinant plant calmodulin and its use to detect calmodulin binding proteins. *Methods Cell Biol* 1995, 49: 487–500.
- Louis-Jeune C, Andrade-Navarro MA, Perez-Iratxeta C. Prediction of protein secondary structure from circular dichroism using theoretically derived spectra. *Proteins* 2012, 80: 374–381.
- Qu B, Yin KQ, Liu SN, Yang Y, Gu T, Hui JM, Zhang L, et al. A highthroughput screening system for Arabidopsis transcription factors and its application to Med25-dependent transcriptional regulation. Mol Plant 2011, 4: 546–555.
- Phean-o-pas S, Limpaseni T, Buaboocha T. Structure and expression analysis of the OsCam1-1 calmodulin gene from Oryza sativa L. BMB Rep 2008, 41: 771–777.
- Grasser KD, Grill S, Duroux M, Launholt D, Thomsen SM, Nielsen VB, Nielsan KH, et al. HMGB6 from Arabidopsis thaliana specifies a novel type of plant chromosomal HMGB protein. Biochemistry 2004, 43: 1309–1314.
- 41. Maurer-Stroh S, Eisenhaber F. Refinement and prediction of protein prenylation motifs. *Genome Biol* 2005, 6: R55.
- 42. Martin SR, Bayley PM. The effects of Ca²⁺ and Cd²⁺ on the secondary and tertiary structure of bovine testis calmodulin. A circular-dichroism study. *Biochem J* 1986, 238: 485–490.
- 43. Maune JF, Beckingham K, Martin SR, Bayley PM. Circular dichroism studies on calcium binding to two series of Ca²⁺ binding site mutants of *Drosophila melanogaster* calmodulin. *Biochemistry* 1992, 31: 7779–7786.

- Grasser KD, Launholt D, Grasser M. High mobility group proteins of the plant HMGB family: dynamic chromatin modulators. *Biochim Biophys Acta* 2007, 1769: 346–357.
- 45. Reeves R. Nuclear functions of the HMG proteins. *Biochim Biophys Acta* 2010, 1799: 3–14.
- Hu CD, Chinenov Y, Kerppola TK. Visualization of interactions among bZIP and Rel family proteins in living cells using bimolecular fluorescence complementation. *Mol Cell* 2002, 9: 789–798.
- 47. Jamshidiha M, Ishida H, Sutherland C, Gifford JL, Walsh MP, Vogel HJ. Structural analysis of a calmodulin variant from rice: the C-terminal extension of OsCaM61 regulates its calcium binding and enzyme activation properties. J Biol Chem 2013, 288: 32036–32049.
- Brokx RD, Scheek RM, Weljie AM, Vogel HJ. Backbone dynamic properties of the central linker region of calcium-calmodulin in 35% trifluoroethanol. J Struct Biol 2004, 146: 272–280.
- Ikura M, Clore GM, Gronenborn AM, Zhu G, Klee CB, Bax A. Solution structure of a calmodulin-target peptide complex by multidimensional NMR. Science 1992, 256: 632–638.
- 50. Kurokawa H, Osawa M, Kurihara H, Katayama N, Tokumitsu H, Swindells MB, Kainosho M, et al. Target-induced conformational adaptation of calmodulin revealed by the crystal structure of a complex with nematode Ca²⁺/calmodulin-dependent kinase kinase peptide. J Mol Biol 2001, 312: 59–68.

- O'Neil KT, DeGrado WF. How calmodulin binds its targets: sequence independent recognition of amphiphilic alpha-helices. *Trends Biochem Sci* 1990, 15: 59–64.
- Rodríguez-Concepción M, Yalovsky S, Gruissem W. Protein prenylation in plants: old friends and new targets. *Plant Mol Biol* 1999, 39: 865–870.
- 53. Krohn NM, Yanagisawa S, Grasser KD. Specificity of the stimulatory interaction between chromosomal HMGB proteins and the transcription factor Dof2 and its negative regulation by protein kinase CK2-mediated phosphorylation. *J Biol Chem* 2002, 277: 32438–32444.
- 54. Banerjee J, Magnani R, Nair M, Lynnette DM, DeBolt S, Maiti IB, Houtz RL. Calmodulin-mediated signal transduction pathways in Arabidopsis are fine-tuned by methylation. *Plant Cell* 2013, 25: 4493–4511.
- Hofmann NR. Calmodulin methylation: another layer of regulation in calcium signaling. Plant Cell 2013, 25: 4284.
- Benaim G, Villalobo A. Phosphorylation of calmodulin. Functional implications. Eur J Biochem 2002, 269: 3619–3631.
- Cooper B, Clarke JD, Budworth P, Kreps J, Hutchison D, Park S, Guimil S, et al. A network of rice genes associated with stress response and seed development. Proc Natl Acad Sci USA 2003, 100: 4945–4950.
- 58. Kwak KJ, Kim JY, Kim YO, Kang H. Characterization of transgenic Arabidopsis plants over expressing high mobility group B proteins under high salinity, drought or cold stress. Plant Cell Physiol 2007, 48: 221–231